RIGA TECHNICAL UNIVERSITY

Ilya Balmages

LASER SPECKLE IMAGE PROCESSING SYSTEM FOR THE ANALYSIS OF LARGE AREA SUBMICRON ACTIVITY

Summary of the Doctoral Thesis

RTU Press
Riga 2025

RIGA TECHNICAL UNIVERSITY
Faculty of Computer Science, Information Technology and Energy
Institute of Applied Computer Systems

Ilya Balmages
Doctoral Student of the Study Program "Computer Systems"

LASER SPECKLE IMAGE PROCESSING SYSTEM FOR THE ANALYSIS OF LARGE AREA SUBMICRON ACTIVITY

Summary of the Doctoral Thesis

Scientific supervisor
Associate Professor Dr. sc. ing.
DMITRIJS BĻIZŅUKS

RTU Press
Riga 2025

Balmages, I. Laser Speckle Image Processing System for the Analysis of Large Area Submicron Activity. Summary of the Doctoral Thesis. – Riga: RTU Press, 2025. – 62 p.

Published in accordance with the decision of the Promotion Council "P-07" of 9 May 2025, Minutes No. 04030-9.7/3.

Cover picture from www.shutterstock.com.

https://doi.org/10.7250/9789934371967
ISBN 978-9934-37-196-7 (pdf)

DOCTORAL THESIS PROPOSED TO RIGA TECHNICAL UNIVERSITY FOR PROMOTION TO THE SCIENTIFIC DEGREE OF DOCTOR OF SCIENCE

To be granted the scientific degree of Doctor of Science (Ph.D.), the present Doctoral Thesis has been submitted for defence at the open meeting of RTU Promotion Council on September 22, 2025 at the Faculty of Computer Science, Information Technology and Energy of Riga Technical University, 10 Zundas krastmala, Room 104.

OFFICIAL REVIEWERS

Professor Dr. sc. ing. Agris Ņikitenko,
Riga Technical University

Ph.D. Viktor Dremin,
Aston University, UK

Ph.D. Mihails Birjukovs,
University of Latvia, Latvia

DECLARATION OF ACADEMIC INTEGRITY

I hereby declare that the Doctoral Thesis submitted for review to Riga Technical University for promotion to the scientific degree of Doctor of Science (Ph.D.) is my own. I confirm that this Doctoral Thesis has not been submitted to any other university for promotion to a scientific degree.

Ilya Balmages …… (signature)
Date: ……

The Doctoral Thesis has been written in English. It consists of an Introduction, six chapters, Conclusions, 65 figures, and three tables; the total number of pages is 121. The Bibliography contains 150 titles.

Abstract

The development of new technologies and data processing algorithms is drawing increasing attention to the field of processing very low-frequency signals. The most well-known applications are aimed at observing “global scale” processes, such as volcano eruptions, mountain-associated waves, earthquakes, and mineral exploration, and require complex equipment. However, there are other industries where very low-frequency signals need to be processed. One of these is monitoring changes in the growth and inhibition of microorganisms. Optical contactless technology (laser speckle patterns analysis) has been proposed for this aim. The technological advantage lies in the small size of compact equipment and change-sensitive granular structure.

The sensitive correlation subpixel algorithm allows the conversion of a speckle image sequence into an array of temporal signals and is capable of highlighting hidden effects. An important advantage of this approach is that any subsequent signal processing algorithms can be applied to the array of obtained signals, such as filtering, operations in the time, frequency, or time-frequency domains, and also use the algorithms of spatial signal processing, analysing the behaviour and changes in the time-spatial domain.

The application of artificial neural networks with additional post-processing based on understanding the properties of the signals has yielded high achievements in the classification of growing (active) and inactive zones.

The research results were applied in the ERDF and LZP projects.

CONTENTS

GENERAL DESCRIPTION OF THE THESIS

Introduction

Very low-frequency signals. Several different technologies have analysed and processed very low-frequency signals (mHz (milliHertz)).

The most common technologies are:

1. Infrasound. Infrasonic waves are sub-audible acoustic waves, typically in the frequency range $0.01 < f < 10$ Hz, and can result from many natural and man-made phenomena. A known example is an international infrasonic monitoring network that is capable of detecting and verifying nuclear explosions. Infrasonic waves can also result from mountain-associated waves, volcanoes, microbaroms, and gravity waves, among others. Infrasound has the ability to reach large distances, ranging from 100 to 500 km.

Low-frequency infrasound (one oscillation in a few seconds) cannot be physically recorded by microphones. In general, infrasound sensor stations consist of an array of sensors that measure pressure variations in the air and consist of many large components.

2. Gravity gradiometry is the field of study of variations or anomalies in the Earth's gravity field via measurements of the spatial gradient of gravitational acceleration. Understanding subsurface anomalies can be used to target oil, gas, and mineral deposits more accurately. The greatest interest lies in the developments of the last decade of airborne gravity gradiometers for gravitational field measurements with improved signal-to-noise and resolution in the bandwidth from 0.001 to 1 Hz.

3. Seismic tomography or seismology. The frequency of seismic waves ranges from fractions of a Hz (mHz) to a few hundred Hz. Normal modes or free oscillations of the Earth are very long-period (very low frequency – mHz) standing surface waves.

4. Magnetotellurics – electromagnetic geophysical method for inferring the Earth's subsurface electrical conductivity. Electric and magnetic fields of Earth are measured over a frequency range 0.1 mHz – 10 kHz. The higher frequency ranges give information on the shallow Earth, whereas deeper information is provided by the low-frequency range.

Very low-frequency signals for analysing spatiotemporal micro-activity. All of the techniques described above require complex equipment and observing global-scale processes. However, there are other industries where very low-frequency signals need to be processed. For example, monitoring changes in growth and inhibition of microorganisms. The growth of microorganisms in space looks like a one-directional progression process. However, microorganisms create many different, multidirectional, random movements on the occupied surface. When considering these processes in the time domain, fluctuations characterizing alternating processes occurring over time are observed. Accordingly, in the temporal frequency domain, frequencies corresponding to these fluctuations (located in the very low-frequency region) can be observed. Spectrogram analysis provides additional insight by allowing simultaneous observation of changes over time and frequency. Thus, temporary signals created by the activity of microorganisms are also very low-frequency signals. This Thesis proposes an optical contactless technology (laser speckle patterns analysis), including signal processing algorithms for monitoring such phenomena.

The technological advantage lies in the small size of compact equipment, change-sensitive granular structure, and the set of image and signal processing techniques to extract useful

information. The application of laser speckle patterns analysis to measure acoustic and seismic signals (in the higher frequency region) has been demonstrated in the literature. Accordingly, potentially, this method can be used for acoustic, seismic, and other applications where processing of very low-frequency signals is required.

Laser speckle patterns technique. The operation of the first laser in 1960 demonstrated that objects viewed in laser light acquire a chaotic granular structure with an irregular pattern, which has no obvious relationship to the macroscopic properties of the illuminated object. The reason is that the surfaces of most materials are extremely rough on the scale of an optical wavelength. When monochromatic light is reflected from such a surface, the optical wave resulting at any distant point consists of many coherent components, each arising from a different microscopic element of the surface, the interference of which results in the granular pattern of intensity that is called “laser speckle”.

It is worth noting that speckle can appear not only from free-space propagation but also within the imaging system.

Initially, the laser speckle effect was only considered a main drawback in using coherent light sources. However, it was later noted that the speckle can also provide useful information. Currently, laser speckle techniques are used in a variety of optical metrology techniques, including displacement, distortion, and strain measurement, surface roughness assessment, velocity measurement, etc. Quite a few of these applications are used in the biomedical field, and in particular in microbiology, to observe microorganisms' development.

Submicron activity analysis. According to available literature, none of the laser speckle-based methods has been focused on 1) microbial growth (colony forming units (CFU) formation) monitoring in early stages; 2) detection and monitoring of differences in microbial activity in different parts of the colony; 3) classification of growing (active)/non-growing (non-active) bacterial colonies or zones; and 4) identifying dynamics and changes of microorganism's activity in the zone of inhibition (around the antibiotic disc).

To monitor these phenomena, in addition to the laser speckle technique, data processing algorithms are widely used. A comparison of the most well-known algorithms for processing speckle patterns was carried out, based on which the advantages of correlation analysis were noted. The application and development of correlation analysis algorithms were analysed, and based on data properties, an approach was proposed, taking into account time and frequency characteristics. The proposed sensitive correlation subpixels algorithm allows the conversion of a speckle image sequence into an array of temporal signals. An important advantage of this approach is that any subsequent signal processing algorithms can be applied to the array of obtained signals, such as filtering, operations in the time, frequency, or time-frequency domains, and also use the algorithms of spatial signal processing, analysing the behaviour and changes in the time-spatial domain.

The application of artificial neural networks with additional post-processing based on understanding the properties of the signals has yielded high achievements in the classification of growing (active) and inactive zones.

The Thesis uses both mathematical simulations and real experiments for algorithm development and data analysis.

The research **aim** is to develop a novel approach for non-contact detection and assessment of submicron activity or growth of submicron objects over a large area, and the ability to classify and evaluate specific submicron objects or events.

To achieve the aim, the following topics have been explored:

1. Development and adaptation of the use of correlation analysis of laser speckle images for submicron activity evaluation.
2. Comparison of the proposed correlation subpixel method with other methods based on the use of laser speckle techniques.
3. Development of tools for monitoring the growth dynamics of a microorganism colony, revealing the migration of activity zones within the colony and comparison with models.
4. Development and demonstration of capabilities of early detection of antibacterial susceptibility in disc diffusion tests using the proposed correlation subpixel method and comparison with models.
5. Classification of active (growing) and non-growing colonies or zones.

The proposed method demonstrated the ability to operate in noisy environments and reveal hidden effects (which were not detected by others described in the literature approaches). The application of artificial neural networks to signals obtained by the proposed algorithm from a sequence of images with additional post-processing has given high achievements in classifying growing (active) and inactive zones, which could not be achieved using raw speckle data.

Actuality

Observation of submicron activity by conventional devices such as microscopes cannot simultaneously cover a large observation area and examine it with high resolution. However, it may be important in many applications, such as the analysis of bacterial or fungal activity in a Petri dish. Therefore, it is necessary to scan the entire area, dividing it into smaller sections beforehand. In cases where the area is relatively large, and the activity changes occur quickly and only in certain places, i.e., the transition from one stage of the field to another takes longer than the scanning period, these changes can be missed. In this case, cameras with an adequate field of view may represent an alternative. It can be used for large field coverage, but it has limited optical resolution, which would not provide submicron resolution for areas above a square centimeter.

Accordingly, there is a need to use other approaches. Recently, the need to perform analysis, data processing, finding, and classification of searched objects or events in a non-contact manner, quickly, with high resolution, and with high quality is becoming more and more frequent. This is especially relevant if direct access to objects is difficult, as objects are small, imperceptible (like a submicron activity), and located in unknown places.

The proposed non-contact optical method is based on laser speckle processing algorithms with high sensitivity, which allows 1) to view the required observation area at the same time without scanning; and 2) the technology is sensitive to submicron movements and changes occurring in the observation field. The method is based on the ability of laser speckle (a specific granular structure) to change the intensity of each speckle (grain) when physical movements occur up to half of the laser wavelength (for example, 0.4 micrometers). On the other hand, the size of the speckle can be a few tens of microns, which allows it to be captured by a typical camera.

Developed and adapted signal processing algorithms will contribute more to the analysis of object activity when movements are minimal (for example, the division of bacteria) or only movements of a specific nature that need to be evaluated.

Thus, even using a low-resolution camera, it is possible to detect submicron activity and perform additional analysis of its parameters and properties significantly earlier than existing methods allow.

Objectives and Hypotheses

The **objectives** of the Thesis:

1. Perform a review of existing methods for processing speckle patterns. Demonstrate the outperformance of the proposed method in the Thesis.
2. Study of correlation analysis techniques of speckle patterns. Comparison of different algorithms, testing execution time, and accuracy. Proposal and adaptation for application to low-frequency signals characterising the activity of microorganisms.
3. Study of the possibility of the proposed method to perform quick and non-contact detection and assessment of submicron activity or growth of submicron objects.
4. Measurement of the spread speed of submicron objects or events in space. Comparison with mathematical models.
5. Study of the possibility of the proposed method to perform the determination of specific hidden phenomena and effects of certain types of submicron objects. Comparison with mathematical models.
6. Demonstrate the ability to classify and evaluate specific submicron objects or events.
7. Publish findings in scientific publications and include them in this Thesis.

During research and development of algorithms of laser speckle image processing for submicron activity evaluation, the following **hypotheses** were defined:

1. The correlation subpixel algorithm is sensitive to small changes caused by activity (in particular submicron activity of microorganisms) and is able to observe/detect them earlier than other widely used methods.
2. The correlation subpixel algorithm for a given type of signal (submicron activity of microorganisms) is more sensitive and provides more information than other widely used algorithms used in the laser speckle technique, such as contrast analysis, speckle size analysis, and decorrelation time analysis.
3. The correlation subpixel algorithm is able to observe/detect activity even when there is no direct vision of it. For example, the formation of colonies in a noisy environment (when the colonies are covered in noise).
4. The correlation subpixel algorithm allows for “emphasizing”/distinguishing the character of activity in the data, thereby providing the opportunity to implement classification based on it.

Research methods

Objectives of the Thesis are accomplished by analytical and experimental research that has been published in the scientific research papers listed in the continuation of this chapter. The

Thesis uses experimental, mathematical, and statistical data analysis, as well as machine learning research methods. Qualitative and quantitative research methods have been used to review the scientific literature and existing and novel methods. Within this research, the primary research subject has been the development of a non-contact optical approach based on laser speckle processing algorithms with high sensitivity for submicron activity observation. Methods for its implementation have also been studied in order to improve the performance and functionality results.

Scientific Novelty of the Thesis

The **scientific novelty** of the Thesis is based on the development and proposal of the system, methods, and algorithms that are aimed at solving practical tasks related to the fast and efficient detection of submicron activity and are able to provide the following:

1) quick and non-contact assessment of submicron activity or growth of submicron objects;
2) the ability to classify and evaluate specific submicron objects or events;
3) measurement of the spread speed of submicron objects or events in space;
4) determination of specific phenomena and effects of certain types of submicron objects.

Practical Significance of the Thesis

The **practical significance** lies in software implementation, experimental validation, and assessment of the discussed methods. The full list of practical achievements is as follows.

1. A review and comparison of methods described in the literature were performed, and the advantages of the proposed method were demonstrated.

2. Results were obtained that could not be observed using a conventional microscope or other non-invasive technology, such as movement of activity in microbial colonies from the center to the edges; classification: active or inactive colony, early detection of the formation of an inhibition zone, detection of fully covered by noise microbial colonies, etc.

3. In practice, the proposed method allows for earlier detection of submicron objects or events (significantly faster than conventional methods).

4. Potential application of the proposed method in practice can be aimed at the following benefits:

4.1. High potential for the development of cost-effective solutions for fast evaluation of bacterial activity in solid media.

4.2. The potential for real-time tracking could revolutionise the way bacteriophage-bacterial interactions are studied, providing empirical data that could complement current experimental data and enhance mathematical models.

4.3. Faster antimicrobial susceptibility results and, therefore, if necessary, faster replacement of empiric antimicrobial therapy with pathogen-targeted therapy, which has greater potential to reduce treatment duration and costs and to reduce mortality.

5. The approach, taking into account parameter adjustment, can be used in different tasks with similar features, for example: 1) monitoring the paint drying process; 2) observation of micro-vibrations; 3) detection of microcracks in the vehicle or aircraft body and identification of various mechanical damages; 4) non-invasive diagnosis of skin diseases; 5) assessment of

blood flow dynamics; 6) detection of objects covered with a thin layer of some material that interferes with direct view; and many other applications, some of which do not yet use the speckle technique, some of which are used, but with different (less sensitive) algorithms.

6. Software implementation has been created in MATLAB.

Approbation

The results of the research were presented at the following international conferences.

1. SPIE Conference 13196, Artificial Intelligence and Image and Signal Processing for Remote Sensing XXX, Edinburgh, Great Britain, 16–19 September 2024.
2. SPIE Conference 13006, Biomedical Spectroscopy, Microscopy, and Imaging III, Strasbourg, France, 7–11 April 2024.
3. SPIE Conference 12628, Diffuse Optical Spectroscopy and Imaging IX, Munich, Germany, 25–29 June 2023.
4. 19th Nordic-Baltic Conference (NBC) on Biomedical Engineering and Medical Physics, Liepaja, Latvia, 12-13 June 2023.
5. SPIE Conference 12572, Optical Sensors, Prague, Czech Republic, 24–26 April 2023.
6. 3rd Baltic Biophysics Conference, Vilnius, Lithuania, 6–7 October 2022.
7. SPIE Conference 12144, Biomedical Spectroscopy, Microscopy, and Imaging II, Strasbourg, France, 7–11 April 2022.
8. SPIE Conference 11920, Diffuse Optical Spectroscopy and Imaging VIII, Munich, Germany, 20–25 June 2021.
9. SPIE Conference 11359, Biomedical Spectroscopy, Microscopy, and Imaging, Strasbourg, France, 6–10 April 2020.

Research results that served as the basis for the Thesis published in the scientific papers

Q1 Journal Articles

1. I. Balmages, J. Liepins, S. Zolins, D. Bliznuks, R. Broks, I. Lihacova, A. Lihachev, "Tools for classification of growing/non-growing bacterial colonies using laser speckle imaging". Frontiers in Microbiology, 14, 1279667, (2023), DOI:10.3389/fmicb.2023.1279667 (**contribution 80 %).**
2. I. Balmages, A. Reinis, S. Kistkins, D. Bliznuks, E. V. Plorina, A. Lihachev, and I. Lihacova, "Laser speckle imaging for visualization of hidden effects for early detection of antibacterial susceptibility in disc diffusion tests", Frontiers in Microbiology, 14, 1221134, (2023), DOI: 10.3389/fmicb.2023.1221134 (**contribution 80 %**).
3. I. Balmages, J. Liepins, E. T. Auzins, D. Bliznuks, E. Baranovics, I. Lihacova, and A. Lihachev, "Use of the speckle imaging subpixel correlation analysis in revealing a mechanism of microbial colony growth," Sci. Rep. 13(1), 2613, (2023), DOI: 10.1038/s41598-023-29809-0 (**contribution 80 %**).

4. I. Balmages, J. Liepins, S. Zolins, D. Bliznuks, I. Lihacova, and A. Lihachev, "Laser speckle imaging for early detection of microbial colony forming units," Biomed. Opt. Express, 12(3), pp. 1609–1620 (2021), DOI: 10.1364/BOE.416456 (**contribution 80 %**).

Conference proceedings

1. I. Balmages, A. Reinis, S. Kistkins, D. Bliznuks, A. Lihachev, I. Lihacova, "Comparison of algorithms for monitoring the behavior of microorganisms based on remote laser speckle method", Proc. SPIE 13196, Artificial Intelligence and Image and Signal Processing for Remote Sensing XXX, 1319611 (2024), https://doi.org/10.1117/12.3032500 (**contribution 50 %**).
2. I. Balmages, A. Reinis, S. Kistkins, J. Liepins, M. Pogorielov, V. Korniienko, K. Diedkova, D. Bliznuks, A. Lihachev, I. Lihacova, "Determination of operating parameters of fungal growth signals analyzed by laser speckle contrast imaging", Proc. SPIE 13006, Biomedical Spectroscopy, Microscopy, and Imaging III, (2024), DOI: 10.1117/12.3016906 (**contribution 50 %**).
3. I. Balmages, D. Bliznuks, A. Reinis, S. Kistkins, E. V. Plorina, A. Lihachev, and I. Lihacova, "Laser speckle imaging-assisted disk diffusion test for early estimation of sterile zone radius", Proc. SPIE 12628, Diffuse Optical Spectroscopy and Imaging IX, 126281Y, (2023), DOI: 10.1117/12.2670618 (**contribution 50 %**).
4. I. Lihacova, I. Balmages, A. Reinis, S. Kistkins, D. Bliznuks, E. V. Plorina, A. Lihachev, "Dynamic laser speckle imaging for fast evaluation of the antibacterial susceptibility by the disc diffusion method", 19th Nordic-Baltic Conference (NBC) on Biomedical Engineering and Medical Physics (2023), DOI: 10.1007/978-3-031-37132-5_39 (**contribution 20 %**).
5. A. Lihachev, I. Balmages, J. Liepins, I. Lihacova, D. Bliznuks, "Dynamic laser speckle imaging for estimation of microbial colony growth in a noisy environment", Proc. SPIE 12572, Optical Sensors 2023; 1257220 (2023), DOI: 10.1117/12.2675953 (**contribution 20 %**).
6. I. Balmages, J. Liepins, E. T. Auzins, A. Zile, D. Bliznuks, I. Lihacova, A. Lihachev, "Evaluation of microbial colony growth parameters by laser speckle imaging", Proc. SPIE 12144, Biomedical Spectroscopy, Microscopy, and Imaging II, 121440B (2022), DOI: 10.1117/12.2621152 (**contribution 50 %**).
7. I. Balmages, J. Liepins, D. Bliznuks, S. Zolins, I. Lihacova, A. Lihachev, "Laser speckle imaging reveals bacterial activity within colony", Proc. SPIE 11920, Diffuse Optical Spectroscopy and Imaging VIII; 1192024 (2021), DOI: 10.1117/12.2615444 (**contribution 50 %**).
8. I. Balmages, D. Bliznuks, J. Liepins, S. Zolins, and A. Lihachev, "Laser speckle time-series correlation analysis for bacteria activity detection", Proc. SPIE 11359, Biomedical Spectroscopy, Microscopy, and Imaging, 113591D (2020), DOI: 10.1117/12.2541663 (**contribution 50 %**).

The results of the Doctoral Thesis research have been used in the following projects

1. Latvian Council of Science project "Fast and non-contact optical estimation of microorganisms activity" (agreement No. lzp-2018/2-0051), 12.2018–12.2020 (employed since August 2019).
2. European Regional Development Fund project "Fast and cost-effective machine learning based system for microorganism growth analysis" (agreement No. 1.1.1.1/19/A/147) (07.2020–06.2023).
3. European Regional Development Fund project "Rapid assessment system of antibacterial resistance for patients with secondary bacterial infections" (No. 1.1.1.1/21/A/034), (2021.01–2023.11).
4. Latvian Council of Science funded project "Dynamic laser speckle imaging for evaluation of fungal growth activity" (agreement No. lzp-2022/1-0247), (2023.01–2025.12).

Structure and Content of the Thesis

The Doctoral Thesis contains an introduction, six main chapters, results analysis, and conclusions. The full Thesis is written in the form of a collection of publications with extended explanations.

The structure of the Doctoral Thesis

The **introduction** validates the topicality of the conducted investigations and formulates the object, the aim, and the research tasks. It describes the scientific novelty and practical significance.

Chapter 1 provides the literature review of non-contact optical measurement methods based on the laser speckle method.

Chapter 2 analyses the development of the laser speckle correlation method and the rationale for its use in estimating submicron activity.

Chapter 3 describes the algorithm's ability to analyse bacterial colonies, with a focus on 1) early detection of bacterial colonies and monitoring growth dynamics, and 2) visualisation of differences in microbial activity over time in different parts of the colony.

Chapter 4 describes the algorithm's ability to early detect antibacterial susceptibility in disc diffusion tests.

Chapter 5 describes the ability to classify between active and inactive colonies (or zones).

Chapter 6 compares the results between the proposed method and other laser speckle methods.

The Results and Conclusions chapter summarises the main contributions of this study and draws conclusions, covers the scientific and practical novelty of the Thesis, and discusses future research directions.

Relationship between aims, topics, and publications

1. Objective 1: Perform a review of existing methods for processing speckle patterns. Demonstrate the outperformance of the proposed method in the Thesis; Conference paper 1; Chapters 1 and 6.
2. Objective 2: Study of correlation analysis techniques of speckle patterns. Comparison of different algorithms, testing execution time and accuracy. Proposal and adaptation for application to low-frequency signals characterising the activity of microorganisms; Journal Article "Correlation analysis techniques of laser speckle images and rationale for its use to assess the growth and behaviour of fungi and bacteria" (in preparation process); Chapter 2.
3. Objective 3: Study of the possibility of the proposed method to perform quick and non-contact detection and assessment of submicron activity or growth of submicron objects; Journal article 4; Conference papers 2, 5, 6, and 8; Chapter 3.
4. Objective 4: Measurement of the spread speed of submicron objects or events in space. Comparison with mathematical models; Journal articles 2 and 4; Conference papers 3 and 4; Chapters 3 and 4.
5. Objective 5: Study the possibility of the proposed method to determine specific hidden phenomena and effects of certain types of submicron objects. Comparison with mathematical models; Journal Article 3; Conference paper 7; Chapter 3.
6. Objective 6: Demonstrate the ability to classify and evaluate specific submicron objects or events; Journal Articles: 1, and "Laser speckle technique for classifying between inhibition and active bacteria growth zones around the antibiotic's discs using a neural network" (in preparation process); Chapter 5.

1. LITERATURE REVIEW OF NON-CONTACT OPTICAL MEASUREMENT METHODS BASED ON LASER SPECKLE TECHNIQUE

This chapter the Doctoral Thesis provides an overview of non-contact optical measurement methods based on the laser speckle technique. The chapter covers the most popular techniques specifically for measuring biological phenomena.

1.1. A brief overview of the discovery and study of the speckle phenomenon

The operation of the first laser in 1960 demonstrated an interesting phenomenon: objects viewed in laser light acquire a granular structure. This granularity bears no obvious relationship to the macroscopic properties of the illuminated object. As it turned out, the surfaces of most materials are extremely rough on the scale of an optical wavelength (about $\lambda = 500(\mathrm{nm})$) [1], [2]. When monochromatic light is reflected from such a surface, the optical wave resulting at any distant point consists of many coherent components, each arising from a different microscopic element of the surface. The speckle can appear not only from free-space propagation but also in imaging systems.

The laser speckle effect was considered a main drawback of using coherent light sources. The optical speckle limits the spatial resolution and decreases the signal-to-noise ratio (SNR). However, it was later noted that the speckle can provide useful information. For example, it is used to measure surface characteristics [3], [4], detect dynamic changes on the surface [5], etc. That is, the changes in the spatial speckle pattern over time can be used to measure the surface's activity.

Obtaining an instantaneous two-dimensional map of velocities or spatiotemporal flow dynamics in real-time is an advantage of the speckle method compared to the Doppler method [6]. Various techniques have been used to characterise bacterial activity in liquid and solid media, such as infrared thermography [7], microcalorimetry [8], flow cytometry [9], and optical coherence tomography [10]. All those techniques require expensive equipment and also well-trained personnel to carry out the experimental work. The dynamic speckle technique is simple and practical, and the analysis based on its principles requires minimal resources. Therefore, this technique has many advantages over others.

The current chapter examines speckle pattern simulations and the most popular methods of laser speckle measurements.

1.2. Speckle patterns mathematics and simulations

The simulation of speckle patterns allows for separate consideration of different processes of observed phenomena – physics, the optical system, and data processing – and making appropriate changes.

The speckle phenomenon results from the superposition of randomly phased elementary components and can be simulated by implementing a numerical model that sums these components on the observation plane [11]. This model can be described using Eq. (1.1).

$$U(x,y) = \frac{1}{\sqrt{N}} \sum_{k=1}^{N} |a_k| \cdot e^{j\varphi_k}, \tag{1.1}$$

where $a_k/\sqrt{N}$ and φ_k is the amplitude and the phase of the kth statistically independent phasor, respectively, and U represents the phasor amplitude of the field. However, the observable quantity is the intensity of a pixel of a speckle pattern, which is acquired with a camera:

$$I(x,y) = \lim_{T\to\infty} \frac{1}{T} \int_{-T/2}^{T/2} |U(x,y;t)|^2 dt \propto U(x,y)U^*(x,y). \tag{1.2}$$

The model described by Eq. (1.1) allows the creation of a static speckle pattern. Another way to create speckle patterns – the distribution intensity at the image plane can be calculated from the Fourier transform by multiplying the light field from the object by the optical pupil function (low pass filter) [12] (Eq. 1.3).

$$I(x,y) = \left| FT^{-1}\left(H \cdot FT\left(e^{j\varphi(x,y)}\right)\right)\right|^2, \tag{1.3}$$

where H represents the circular aperture of the camera lens, and FT and FT^{-1} are the direct and inverse Fourier transforms, respectively.

Both simulation methods provide similar patterns (Fig. 1.1). It becomes evident that by the 1st method, the implementation time is significantly longer.

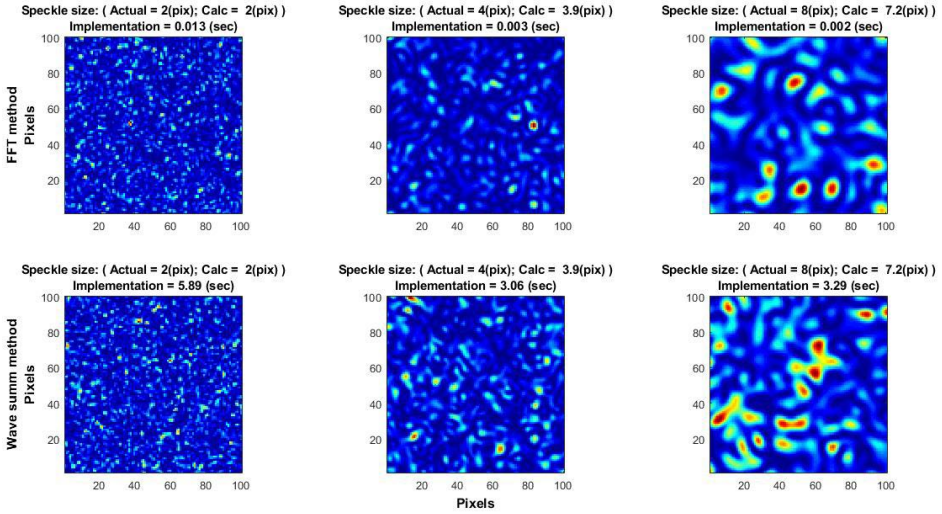

Fig. 1.1. Static simulation of speckle images. Top row: using the Fourier transform. Bottom row: using the sum of the waves. The speckle sizes increase from left to right: 2, 4, 8 (pix).

Dynamic speckle is a phenomenon that occurs when laser light is scattered by objects that exhibit some kind of activity. The model takes into account that activity occurs on a rough surface that changes the microstructure, but its reflectivity is maintained constant. The variation of the microtopography is added to the phase [13]. The study [14] describes the process of creating continuous phase trajectories between two given limits so that the evolution of the speckle pattern is also continuous.

Two sets of statistically independent random numbers with a uniform distribution are created to implement this process. With the Box–Muller transformation from these two sets, two new sets of random variables are created, also statistically independent, but with a Gaussian distribution:

$$Y_1 = \mu + \sigma \cdot \sqrt{-2\ln(X_1)} \cdot \cos(2\pi \cdot X_2); \quad Y_2 = \mu + \sigma \cdot \sqrt{-2\ln(X_1)} \cdot \sin(2\pi \cdot X_2). \tag{1.4}$$

The μ, σ values can be determined: $\mu = 0, \sigma = 1$, and the following procedure can berealized:

$$\begin{vmatrix} Z_1 \\ Z_2 \end{vmatrix} = \frac{1}{\sqrt{2}} \cdot \begin{vmatrix} 1 & -1 \\ 1 & 1 \end{vmatrix} \begin{vmatrix} \sqrt{1+r} & 0 \\ 0 & \sqrt{1-r} \end{vmatrix} \begin{vmatrix} Y_1 \\ Y_2 \end{vmatrix} \tag{1.5}$$

Two sets of random numbers are obtained: bivariate normal with correlation coefficient *r*. The next step uses the percentile transformation:

$$T_1 = F_z(Z_1),\ T_2 = F_z(Z_2)\ , \tag{1.6}$$

where the normal cumulative distribution function is written as F_z.

Two sets of random numbers are obtained with a uniform distribution on the unit interval. The new sets are no longer statistically independent. Sets T_1 and T_2 are brought into the phase:

$$\varphi_n(x, y) = 2\pi T_n. \tag{1.7}$$

Then, two speckle patterns are created using Eq. (1.5). To get speckle patterns with an arbitrary degree of polarisation, the two resulting speckle patterns are averaged [15]:

$$I(x, y) = \frac{I_1(x, y) \cdot (1 + p) + I_2(x, y) \cdot (1 - p)}{2}, \tag{1.8}$$

where $0 < p < 1$, is the degree of polarisation. The new probability density function becomes the Rayleigh distribution. This behaviour corresponds to a real physical process [16]. The speckle images generated by this method [14] change smoothly from frame to frame (Fig. 1.2).

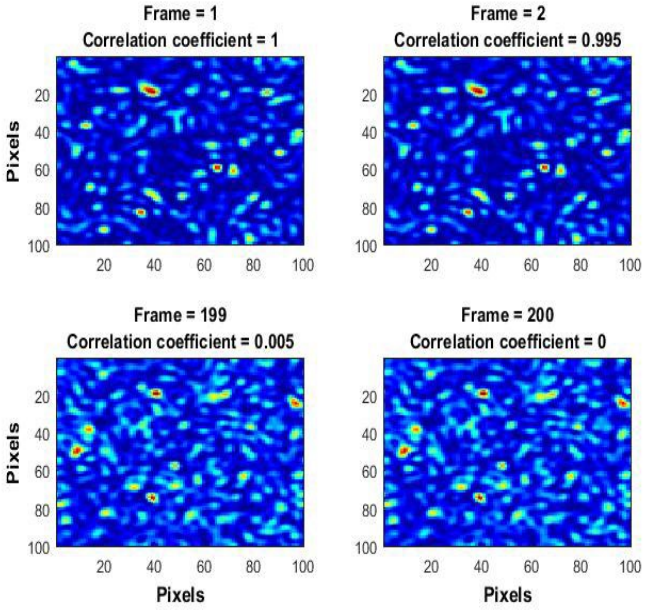

Fig. 1.2. The first two frames (top) and the last two frames (bottom) in a sequence of speckle images, with a correlation coefficient smoothly changing from 1 to 0.

Adding a contribution from biological models of submicron activity behavior will provide a full simulation of the phenomena being studied.

1.3. The speckle size

The speckle size carries information on the scattering media. For example, it can be used to measure the roughness of a surface [17]. The average speckle size of the imaging systems with lens is given by [18]:

$$S \approx 1.2\lambda(1+M)\frac{f}{\alpha}, \tag{1.9}$$

where M is the magnification and f/α the F-number of the lens (focal length over aperture). The average speckle size is estimated as the normalised autocovariance function of the intensity speckle pattern acquired in the observation plane [19]. Using the Wiener–Khinchin theorem [20], it is possible to obtain a faster formula operating in the frequency domain:

$$c_I(x,y) = \frac{FT^{-1}\left\{\left|FT\left[I((x,y)\right]\right|^2\right\} - \left\langle I(x,y)\right\rangle^2}{\left\langle I(x,y)^2\right\rangle - \left\langle I(x,y)\right\rangle^2}, \tag{1.10}$$

where $I(x, y)$ is the intensities in the observation plane (x, y), FT, FT^{-1} the direct and inverse Fourier transform and $\langle\ \rangle$ corresponds to a spatial average.

The average speckle size may be estimated by the full width at half maximum (FWHM) of the autocovariance function. Thus, if the speckle size is unknown, it can be calculated from the speckle image.

1.4. The speckle contrast parameter

Another important parameter in speckle measurements is contrast (K) [21].

$$K = \frac{\sigma}{\langle I\rangle} = \frac{\sqrt{\langle I^2\rangle - \langle I\rangle^2}}{\langle I\rangle}, \tag{1.11}$$

where $\langle I\rangle$ is the spatial mean intensity and σ is the spatial standard deviation of intensity. The lower values of K correspond to more intense dynamic changes in the observed medium. This property of the speckle interference effect is useful for its application in the biomedical field [22].

1.5. Decorrelation time analysis

The Thesis demonstrates the relationship between contrast, exposure time and decorrelation time. Study [16] demonstrates that taking into account the finite number of samples to be used, the following correlation formula was obtained:

$$C_t(k*\delta t, x, y) = \frac{\langle I(t,x,y)I(t+k*\delta t)\rangle - \langle I(t,x,y)\rangle\langle I(t+k*\delta t)\rangle}{\sqrt{[\langle I^2(t,x,y)\rangle - \langle I(t,x,y)\rangle^2][\langle I^2(t+k*\delta t,x,y)\rangle - \langle I(t+k*\delta t,x,y)\rangle^2]}}, \tag{1.12}$$

where (x, y) are the pixel positions, k is the frame number, and δt is the time interval between two adjacent frames.

This expression is used for decorrelation time or rate analysis [23], [24]. The decorrelation time is when the correlation between the original image and the subsequently acquired images

is reduced to 50 %. For biological specimens, study [16] proposes to use (1/e = 0.368). One of the reasons decorrelations occur is that the light is scattered from many individual moving scatterers, such as particles in a media. Observing dynamic events, the temporal correlation decreases.

1.6. Chapter conclusions

In this chapter, speckle pattern simulations and speckle pattern parameters for dynamic events analysis (suitable also for the medical/biological field) were considered; there is a relationship between all of them with correlation analysis. Thus, it becomes clear that correlation analysis is an important, powerful, and promising tool for analyzing speckle patterns (also in the medical/biological field). The next chapter will consider the development of correlation analysis for laser speckle images and the rationale for its use for submicron activity evaluation.

2. A REVIEW OF THE DEVELOPMENT OF CORRELATION ANALYSIS OF LASER SPECKLE IMAGES AND THE RATIONALE FOR ITS USE FOR SUBMICRON ACTIVITY EVALUATION

Based on the stated aim and tasks, the second chapter of the Doctoral Thesis performs an overview of the development of correlation analysis (signal processing algorithms with high sensitivity) of laser speckle images and the rationale for its use for microbiological data and submicron activity evaluation as a research object.

2.1. Introduction to the chapter

Correlation analysis can provide more accurate information about displacements than contrast analysis, allowing more sensitive monitoring of moving dynamic events or objects [25]. Correlation algorithms have found wide application in mechanics, acoustics, and, to a much lesser extent, microbiology. The current chapter reviews the evolution of correlation analysis techniques of laser speckle images and a rationale for their use in assessing fungal and bacterial growth and behaviour.

2.2. Speckle-displacement measurement

The first computer-based digital image speckle correlation system was presented in the early 1980s to analyse mechanical deformations [26], [27]. The speckle correlation method enables the determination of small deformations, even with overlaying large, rigid body motions. The cross-correlation algorithm compares the sub-images (from the reference and shifted images) and finds a displacement (Eq. (2.1)).

$$CC(u,v) = \sum_x \sum_y \Big(\big(a(x,y)\big) * \big(b(x-u, y-v)\big) \Big), \tag{2.1}$$

where $a(x,y)$ and $b(x,y)$ are two frames (before and after deformation), u and v is spatial displacement between two frames in the directions of x and y, respectively.

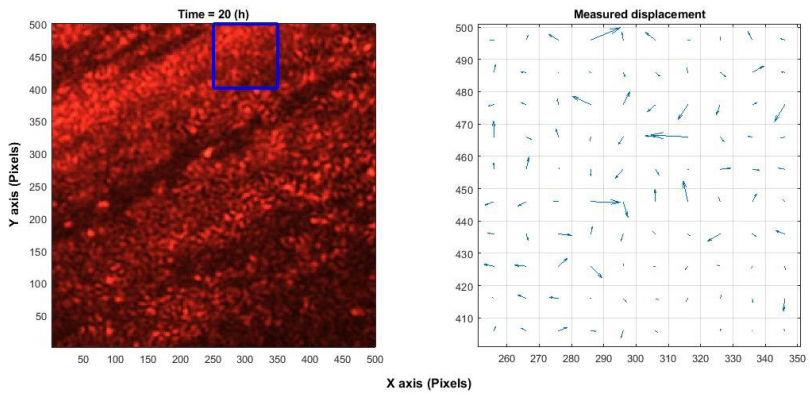

Fig. 2.1. Experiment with the fungi *Candida albicans*: right – a speckle image for a time of 20 h from the beginning of the experiment; a square of 100 pixels by 100 pixels is highlighted in blue; left – displacement field between two frames (1 s); a speckle image of 100 pixels by 100 pixels is divided into blocks of 10 pixels by 10 pixels (100 blocks).

The full version of the Thesis demonstrates a simulation of the mechanical shift (all object sections are shifted in the same direction). A similar analysis was performed using the *Candida albicans* fungi to compare how a simple shift differs from the behaviour of fungi (Fig. 2.1).

2.3. Signal reconstruction by zero-mean normalised cross-correlation between images

In laser speckle processed audio signals, there is only speckle movement in the plane (*xy*) between frames, but no shape change [28]. In the first (reference) image, a template (N×N pixels) is selected. By zero-mean normalised cross-correlation (Eq. (2.2)), a larger area is scanned in the next-in-time ("deformed") image to locate the template position and determine the displacement.

$$ZNCC(u,v) = \frac{\sum_x \sum_y \left((a(x,y)-\overline{a}) * \left(b(x-u,y-v)-\overline{b} \right) \right)}{\sqrt{\sum_x \sum_y (a(x,y)-\overline{a})^2 * \sum_x \sum_y (b(x-u,y-v)-\overline{b})^2}}, \quad (2.2)$$

where $a(x,y)$ is a part of the first (template) frame and $b(x,y)$ is a part of the next frames in a sequence, $\overline{a}$ and $\overline{b}$ are the average values of these frame parts. This procedure is carried out with every speckle image until the end of the experiment [29], [30]. The full version of the Thesis demonstrates the simulation of reconstructing an acoustic signal.

2.4. Sequence of laser speckle images of microorganisms' activity converted into time signals

In the case of fungi or bacteria, due to the activity of microorganisms, the speckle pattern will not only be displaced in space but will also change over time from frame to frame (Fig. 2.1). For this reason, it is necessary to perform a correlation with each pair of consecutive images: 1 with 2, 2 with 3, etc. (In Eq. (2.2), $a(x,y)$ and $b(x,y)$ will be the two adjacent frames in the sequence). To take this into account when reconstructing the signal, the previous displacements are accumulated (Eq. (2.3)).

$$sig[n] = \sum_{i=1}^{n} \hat{\delta}[i], \quad (2.3)$$

where $\hat{\delta}$ is all previous displacements.

Furthermore, the bacteria create weak micro-vibrations that cannot shift the image by several pixels in a short time interval. Accordingly, it is necessary to concentrate on the same position without scanning. To obtain signals over the entire field, it is necessary to divide it into N×N pixels, and in each of these sections, ZNCC (and interpolation) between successive frames will be performed. Figure 2.2 compares the reconstructed signal within the bacterial and fungal colonies and outside them.

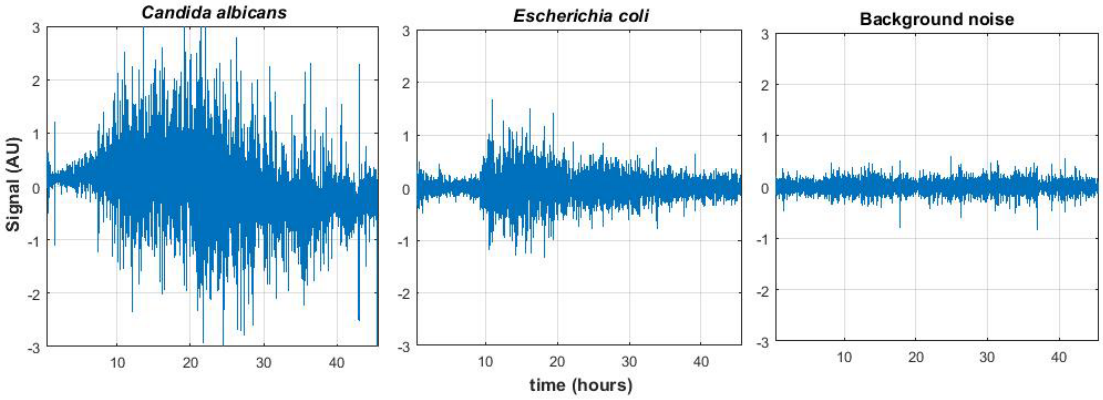

Fig. 2.2. The signal obtained using the algorithm: left – a signal from a *Candida albicans* (fungi) colony; centre – a signal from an *E. coli* (bacteria) colony; right – a signal out of colony.

2.5. Measurement accuracy and algorithm implementation time

This subsection discusses several methods for implementing the cross-correlation algorithm, ensuring both high accuracy on the one hand, and being fast on the other. The main advantage of the normalised cross-correlation over the non-normalised is that it is less sensitive to linear changes in the amplitudes of the two compared signals [31]. On the other hand, non-normalised cross-correlation is faster.

In addition to ZNCC, normalised cross-correlation (NCC) was used, which is similar to ZNCC but without subtracting the means of the images [32] (Eq. (2.4)). Due to the subtraction of the local mean, the ZNCC provides better robustness than the NCC since it tolerates uniform brightness variations as well.

Consider several implementation options and compare them: first and most importantly, in terms of accuracy (Fig. 2.3) and then in terms of processing time (Tables 1 and 2).

1) Normalised cross-correlation (NCC):

$$NCC(u,v) = \frac{\sum_x \sum_y \left((a(x,y)) * (b(x-u,y-v)) \right)}{\sqrt{\sum_x \sum_y (a(x,y))^2 * \sum_x \sum_y (b(x-u,y-v))^2}}. \quad (2.4)$$

2) The implementation of ZNCC follows Eq. (2.2).

3) To reduce the computation time, it is worth implementing the algorithm in the frequency domain. One approach is to implement phase correlation, which is normalised [33] (Eq. (2.5)). This method will work much faster, but the result will be different from the implementation of zero mean normalised cross-correlation (Eq. (2.2)).

$$PC(u,v) = FT^{-1}\left(\frac{[FT[a((x,y)] * FT[b((x,y)]^*]}{|FT[a((x,y)] * FT[b((x,y)]|} \right), \quad (2.5)$$

where FT^{-1} and FT is inverse and direct Fourier transform, and $()^*$ is complex conjugate.

4) In the study of J. P. Lewis [34], an algorithm is presented that, after a known finding of a fast non-normalised cross-correlation in the frequency domain, allows it to be converted into a normalised. The accuracy is the same as the ZNCC. This method was apparently designed to work with relatively large matrices, where the implementation is quite fast; however, for small

matrices, for example, 10 pixels by 10 pixels, the normalistion process is slow, and this method will be quite a bit faster than the ZNCC, but much slower than phase correlation.

5) Another implementation option proposed by us: the average is subtracted from the speckle images, and then the images are normalised. Then, frequency domain correlation is performed with two normalised images (according to the formula for non-normalised frequency domain cross-correlation) (Eq. (2.6)). The accuracy is the same as in the ZNCC or in the previous method (by J. P. Lewis). The processing time is comparable (slightly slower) to phase correlation.

$$An(x,y) = \frac{a(x,y)-\overline{a}}{\sqrt{\sum_x \sum_y (a(x,y)-\overline{a})^2}}\ ;\ Bn(x,y) = \frac{b(x,y)-\overline{b}}{\sqrt{\sum_x \sum_y (b(x,y)-\overline{b})^2}}\ ; \qquad (2.6)$$

$$ZNCC(u,v) = FT^{-1}([FT[An((x,y)] * FT[Bn((x,y)]^*]).$$

6) If the speckle images are large in size, not 10 pixels by 10 pixels, but for example, 100 pixels by 100 pixels or more, then to calculate the ZNCC, the formula in the time domain (Eq. (2.2)) can be used. However, do not use all the shifts, but only a couple in the central part (to obtain a correlation peak only), for which the interpolation is made. If the images are large in size, then the method will be a faster implementation than in the frequency domain. For small sizes in the frequency domain, it is slightly faster.

Figure 2.3 shows the results of different correlation functions (correlation between two frames shifted by a non-integer number of pixels (0.5 pixels) along each axis). In this case, the result will either not be shifted or shifted by 1 pixel, and only subpixel interpolation can find a more accurate value. The results of all algorithms were compared with the original implementation (ZNCC). It can be seen that already in this case, with a small displacement, the phase correlation and NCC show differences from the original, while the implementations in the frequency domain according to the Lewis method and the proposed method by the current study, show closeness to the original.

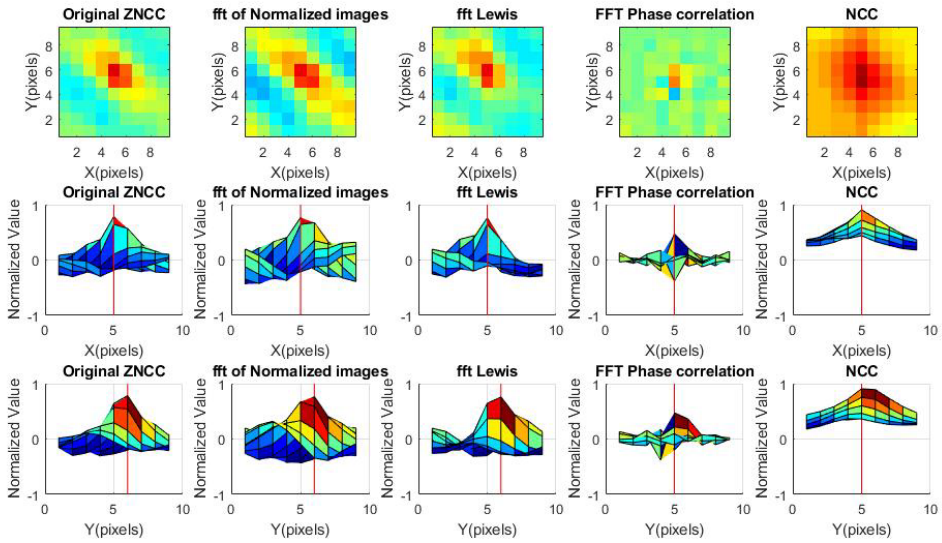

Fig. 2.3. Comparison of different correlation functions. The results of correlating a frame with a frame shifted by 0.5 pixels. Deviations from the reference method are visible. The performance of phase correlation worsened.

Thus, if the images are shifted or deformed, the performance of the phase correlation drops (both accuracy and peak value), while in both the time and frequency domains, the performance of ZNCC remains high.

Below are tables that describe the processing time for different algorithms. The results are obtained statistically.

Table 1

The differences in processing time for different algorithms. The section size of the speckle image is 10 pixels by 10 pixels

Speckle image section size = 10 pixels × 10 pixels	**NCC, Eq. (2.4)**	**Original ZNCC, Eq. (2.2)**	**ZNCC uses only 3 shifts around the peak**	**Lewis method**	**Phase correlation, Eq. (2.5)**	**Frequency domain correlation of normalised images, Eq. (2.6)**
Average (μs)	515.9	550.0	93.9	545.5	48.0	81.8
Standard deviation (μs)	117.3	150.4	82.7	78.5	34.7	64.9

Table 2

The differences in processing time for different algorithms. The section size of the speckle image is 100 pixels by 100 pixels

Speckle image section size = 100 pixels ×100 pixels	**NCC, Eq. (2.4)**	**Original ZNCC, Eq. (2.2)**	**ZNCC uses only 3 shifts around the peak**	**Lewis method**	**Phase correlation, Eq. (2.5)**	**Frequency domain correlation of normalised images, Eq. (2.6)**
Average (ms)	473.8	476.8	0.9	13.0	1.3	1.1
Standard deviation (ms)	30.5	27.4	0.1	1.4	1.5	0.2

2.6. Chapter conclusions

The methods for detecting mechanical vibrations and reconstructing audio signals were the motivation for employing the technique described in this chapter. The movement of fungi and bacteria is chaotic, which causes not only image displacements but also changes in the images themselves. For this reason, in the case of microorganisms, comparisons occur between each pair of consecutive frames (and not with a template). The resulting shifts are accumulated to ensure the continuity of the signal.

Various methods for implementing normalised cross-correlation were considered. Accuracy and performance time have been analysed, and based on them, the optimal method was selected.

3. CORRELATION SUBPIXEL ANALYSIS OF LASER SPECKLE IMAGES FOR MONITORING THE DYNAMICS OF THE COLONY OF MICROORGANISMS GROWTH AND REVEALING THE MIGRATION OF ACTIVITY ZONES WITHIN THE COLONY

Based on the stated aims and tasks, Chapter 3 of the Doctoral Thesis describes in more detail the proposed analysis method and its application for microbiological data and submicron activity evaluation as a research object. The chapter covers experimental confirmation of the capabilities of earlier detection of submicron activity and the efficiency of growth models of submicron events.

3.1. Laser speckle imaging system

The system was assembled to capture macro-scale images under white light and laser illumination. The system's main components are presented in Fig. 3.1. The speckle images were captured by a CMOS camera with 1–30-second intervals (depending on the microorganism types) for experiments with different durations (10–110 hours). According to the available literature, the illumination conditions applied in the current research are optimal and do not affect microbial growth [35]. White light experiments were performed separately from the laser speckle imaging by using the same setup. The images were taken every 15 minutes. The full version of the Thesis demonstrates a more detailed system description.

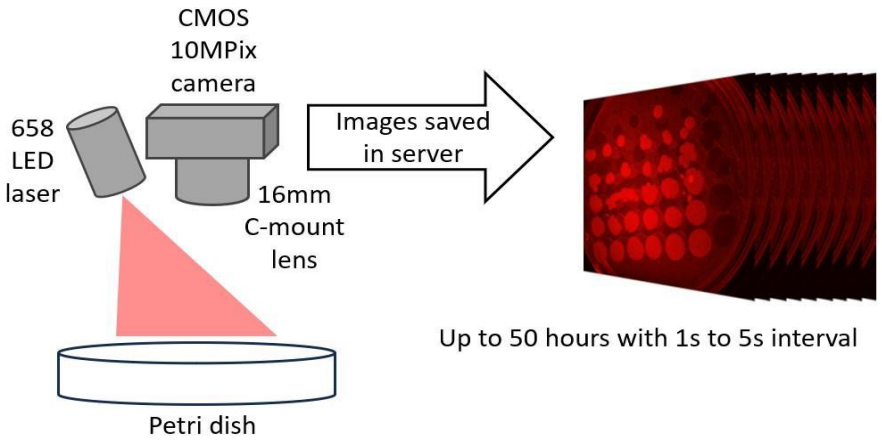

Fig. 3.1. Setup scheme for burst image capturing of bacteria growing process under 658 nm laser illumination.

3.2. Challenge of early detection of bacterial colonies and monitoring growth dynamics

Determination of the viable microbial cells in a sample is one of the central tasks of epidemiology. Each viable cell initiates the development of one colony on an agar plate medium, referred to as a colony-forming unit (CFU). A limitation of this method is the need to wait until colonies reach a certain size before they can be detected. Currently, counting microorganisms in the early stages of colony formation is possible only with a microscope, which is limited to a small sample area. Automated counting of colony size increase dynamics is possible only by using regular cameras that are limited in optical resolution and, therefore, can detect signs of microbial colonies only after a certain size threshold is reached. It would take 8–22 h for the colony to reach the size of 0.2 mm, the detection limit for a photo camera. In standard methods, the waiting time is 18–40 hours for CFUs to "develop" before counting them [36].

One of the options for the fast and early evaluation of microorganisms' activity is a non-contact optical technique called laser speckle patterns analysis. The growth of bacterial colonies on the surface leads to changes in scattering properties, and consequently, the speckle pattern and the behaviour of the acquired image also vary [11]. According to available literature [37]–[44], none of the laser speckle-based methods have focused on monitoring microbial growth (CFU formation) in the early stages. The current chapter will prove that dynamic laser speckle image analysis methods can be used to detect the CFU of different microbes in solid media.

3.3. Challenge of visualisation of differences in microbial activity over time in the different parts of the colony

The microbial growth on the edge of the colony is more active than in its centre due to the constant supply of nutrients from the surrounding media or the constant push of the cells on the lateral ones. Different microbial activities within colonies can be explored only with invasive procedures, such as colony cross-sectioning and viability staining [45].

The proposed speckle analysis system is capable of recording the growth of a microbial colony and visualising microbial growth activity in the different parts of the colony. This method was tested on three different microorganisms: *Vibrio natriegens, Escherichia coli*, and *Staphylococcus aureus*, confirming the accuracy of previous models of colony growth and providing a methodology for microbial activity analysis within colonies.

3.4. Converting subsequent frames of speckle images into a time signal

The current subsection provides a description of the correlation analysis of laser speckles in more detail. Chapter 2 describes how the correlation method can be used to convert the change between subsequent frames into a temporal signal. By analysing this signal, it is possible to detect events caused by the vibration of the measured surface or activity on it. For example, the dynamic spreading of a bacterial colony.

A method for speckle image conversion into a time signal is described below.

1) A two-dimensional normalised correlation between two adjacent frames in a sequence is performed. This allows for the detection of changes between them because of dynamic activity. (Canonical Equation (2.2) or faster Equation (2.6) in Chapter 2).

2) Changes that occur between successive frames are characterised by an offset in the location of the maximum correlation value (Eq. (3.1)).

$$\left(\hat{u},\hat{v}\right) = \arg\max_{u,v}\left(Corr(u,v)\right), \tag{3.1}$$

where u and v are spatial displacements between two adjacent frames in a sequence in the directions of x and y, respectively.

3) The offset between successive frames does not represent the integer number of pixels. For this reason, interpolation was performed within the maximum of the correlation function [46]. This was performed separately for the x-axis and the y-axis. Equation (3.2) shows the parabolic interpolation for the x-axis.

$$\hat{\delta}_x = -\frac{b_u}{2a_u} = \frac{\hat{Corr}(\hat{u}-1,\hat{v}) - \hat{Corr}(\hat{u}+1,\hat{v})}{2\left(\hat{Corr}(\hat{u}-1,\hat{v}) - 2\hat{Corr}(\hat{u},\hat{v}) + \hat{Corr}(\hat{u}+1,\hat{v})\right)}, \tag{3.2}$$

where a_u and b_u are the coefficients of the parabola.

4) Offsets obtained between each pair of adjacent samples were accumulated (separately for x and y axes) to consider previous offsets (Eq. (2.3) in Chapter 2).

Running the described algorithm for consecutive N × N-pixel images for the entire sequence creates a "time signal". To avoid the influence of local transient spikes, smoothing the signal [47] is expedient (obtain signal envelope). A moving root-mean-square technique can be used for this purpose:

$$Env[n] = \sqrt{\frac{1}{N}\sum_{k=n-N+1}^{n} sig[k]^2}, \tag{3.3}$$

where N is the length of the window, n is the current sample, and k is the index running inside the window. An increase in signal values will be observed when bacterial growth occurs.

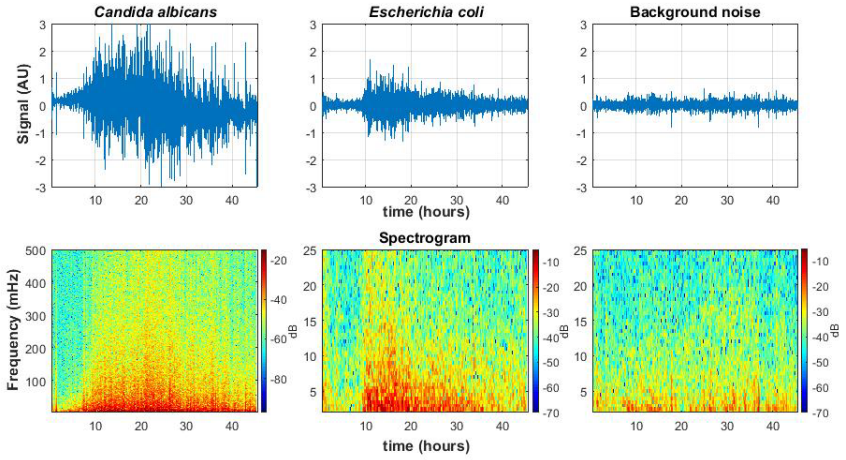

Fig. 3.2. Top: The signal obtained using the algorithm (signal from the colony centre). The left column shows a signal from *Candida albicans* fungi; a similar speckle signal pattern was observed also for *Aspergillus niger* fungi. The centre column shows a signal from an *E. coli*

bacterial colony; a similar speckle signal pattern was also observed for *S. aureus* and *V. natriegens* bacteria. Bottom row: A spectrogram is a representation of a signal in a time-frequency domain using a short-time Fourier transform (STFT), allowing the simultaneous observation of the behaviour of the signal and noise in time and frequency. Right side: the noise (outside the colony) obtained using the algorithm (top) and noise spectrogram (bottom).

In Fig. 3.2, it is possible to compare the signal (inside the colony) and the noise (outside the colony). The signal is much higher than the noise level. The bottom row represents the spectrograms [48].

The signal characterising the activity of bacteria is located in the low-frequency range from 0 to 15–25 mHz. From a practical point of view, this means that according to the Nyquist–Shannon sampling theorem [49], [50], the sampling frequency between frames must be at least 50 mHz, that is, the frame at least once every 20 seconds (Eq. (3.4)):

$$t_s = \frac{1}{f_s} \geq \frac{1}{(2 \times f_{\max})}, \tag{3.4}$$

where t_s is the time between frames (in seconds), accordingly, f_s is the sampling frequency, and $f_{\max}$ is the maximum frequency of the useful signal (in Hz).

Experiments conducted with the fungi *Aspergillus niger* and *Candida albicans* showed that the signal is in the frequency range from 0 to 150 mHz. Accordingly, the sampling frequency between frames must be at least 2 × 150 mHz, that is, a frame at least once every 3.33 seconds (Fig. 3.2).

3.5. Operations in a noisy environment

Real systems must operate in various environments, with an unknown level of noise. To analyse the algorithm's performance in a noisy environment, a bacterial colony detection experiment was performed using the laser speckle technique with noise added. A high noise level was set in the experimental field (3–4 times higher than normal background noise). Figure 3.3 shows an example of three bacterial colonies developing in a noisy environment. On raw speckle images (top row), the colonies are not visible at all. Using the subpixel correlation algorithm (which involves displacement finding using correlation and refining using subpixel interpolation), all three colonies will be detected (bottom row), and their evolution over time can be observed.

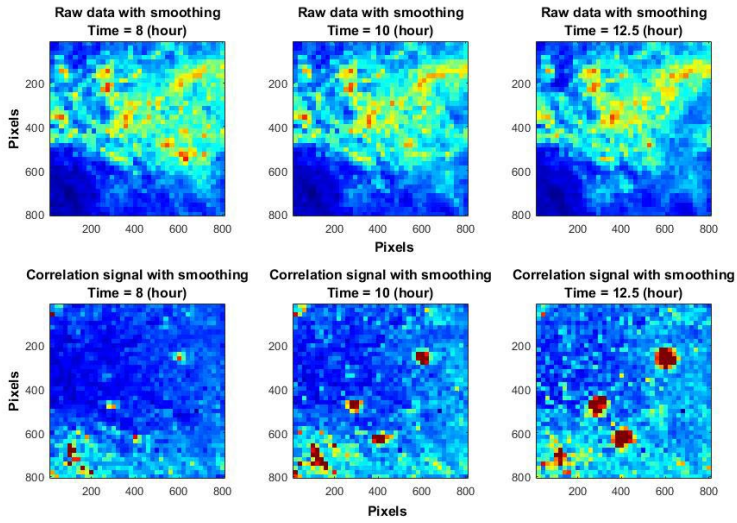

Fig. 3.3. Raw laser speckle images with smoothing of V. natriegens sample at 8 h, 10.5 h, and 12.5 h (top row) and correlation signal with smoothing obtained using subpixel analysis at 8 h, 10 h, and 12.5 h (bottom row).

3.6. Early detection of microbial colony forming units

3.6.1. Analyses of colony growth under white light illumination

Microbial growth on the agar surface and formation of a colony is a self-limiting process that starts with the maximum rate, which is gradually inhibited by exhaustion of necessary nutrients, accumulation of end products of microbial metabolism. There are many mathematical models describing microbial colony growth; among them, the Gompertz model is one of the common [51], [52] (Eq. (3.5)).

$$\mu(t) = \mu_0 \times e^{-\mu_i(t-t_0)}, \tag{3.5}$$

where μ is specific growth rate (h^{-1}), μ_0 is specific growth rate at the beginning of colony formation (h^{-1}), μ_i is specific growth rate at infliction (or specific inhibitory rate), t_0 represents the time at the beginning of the colony growth and t is the actual time (h).

Equation (3.6) describes the growth of the colony radius as a function of time.

$$r(t) = r_{\max} \times e^{-\left(\ln\left(\frac{r_{\max}}{r_0}\right)\times e^{-\left(\mu_i\cdot(t-t_0)\right)}\right)} \tag{3.6}$$

Equation (3.6) shows the growth of the colony radius, where $r_{\max}$ is the maximal radius that the colony can reach in the given environmental conditions, r_0 is the initial radius at t_0, and μ_i is the specific growth rate at the inflexion point of the area curve. Over time, gradual inhibition of colony growth occurs, which can be described by μ_i. To use these equations to simulate the growth of real CFU, μ_0 and μ_i should be found. Data under white light illumination (bacteria *Vibrio natriegens*) were taken as a reference. Using Eq. (3.6), the μ_i for *V. natriegens* was calculated at given temperature and media conditions (Fig. 3.4).

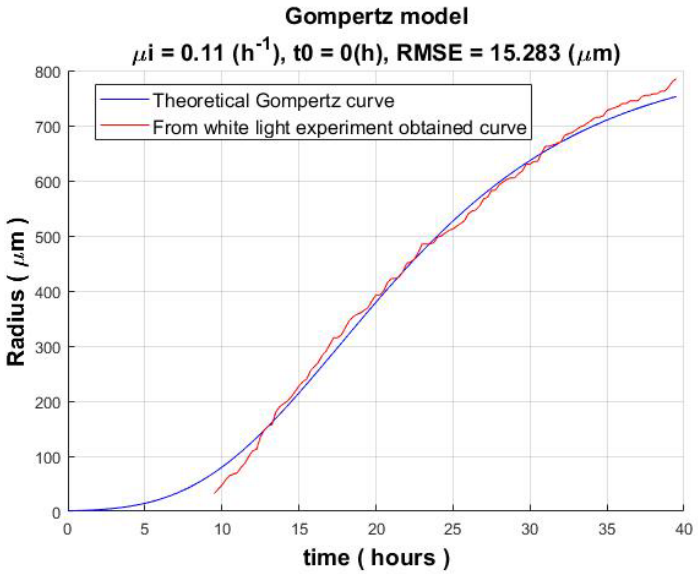

Fig. 3.4. The growth dynamics of *V. natriegens* colony. Theoretical Gompertz-curve (blue) and experimental curve (red) of *V. natriegens* colony radius dynamics over time.

The μ_i is not a fixed number. This coefficient characterises the decrease in the colony growth rate over time. Usually, the μ_i can vary by 20–50 % among the same organism [51]. To extract parameters from the given experimental data set, a parameter scan was used. As a criterion, the root mean square error (RMSE) to minimize Eq. (3.7) to find μ_i and t_0 was used.

$$RMSE = \sqrt{\frac{1}{n}\sum_{i=1}^{n}\left(R_{\text{Gompertz}}[i] - R_{\text{measured}}[i]\right)^2}, \tag{3.7}$$

where R_{Gompertz} is the radius estimated from the Gompertz model, R_{measured} is the radius determined experimentally, and n is the number of measurement points.

3.6.2. Analyses of colony growth by processing laser speckle images

For the speckle image, analysis of *V. natriegens* colony growth was performed using a subpixel correlation algorithm. Using the scanning method for several parameters (growth rate, growth start time, and maximum radius of colony), it is possible to obtain the most optimal suitable Gompertz curve in which the root mean square error (RMSE) value will be minimal (Fig. 3.5).

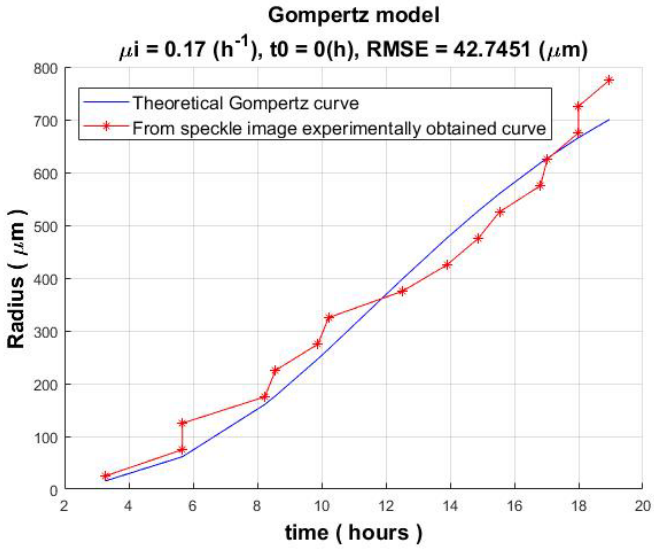

Fig. 3.5. *Vibrio natriegens* colony radius obtained by speckle image experiment (red) and theoretical Gompertz curve (blue). Interestingly, the first signals above the threshold level from speckle imaging can be extracted as quickly as within three hours from the beginning of the cultivation.

3.6.3. Comparison of colony growth measurements in white light and speckle imaging experiments

Comparing these two techniques, it was obtained that with the speckle imaging technique, it is possible to detect microbial activity earlier than using white light imaging (Fig. 3.6).

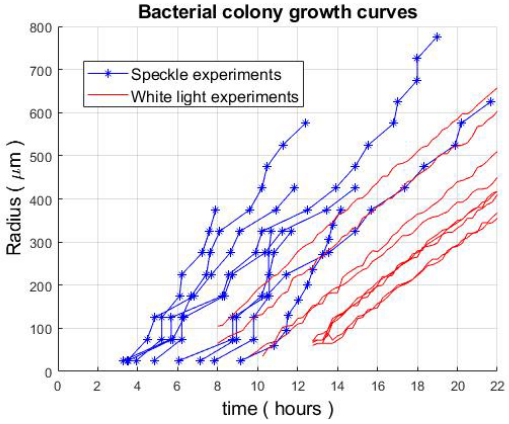

Fig. 3.6. Comparison of growth curves of a colony of bacteria, *Vibrio natriegens,* measured by analysis of laser speckle images and visual examination under white light illumination.

For other bacteria, not only for *Vibrio natriegens*, as well as for *Escherichia coli* and Staphylococcus aureus bacteria, the comparison results were similar.

3.7. Correlation subpixel analysis for determining spatiotemporal activity patterns during colony growth

3.7.1. Detection of high microbial activity zones using the laser speckle imaging system

The correlation subpixel signal characterises bacterial activity in the colony, increasing, reaching its maximum, and then decreasing.

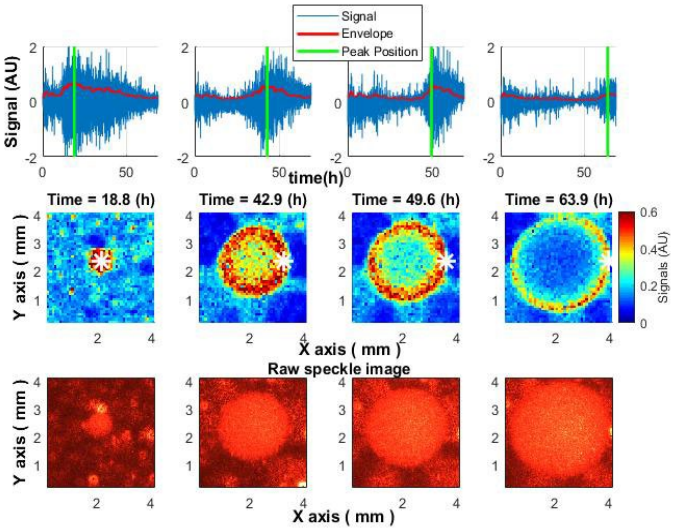

Fig. 3.7. Spatiotemporal distribution of the speckle signal across the *S. aureus* colony. Upper row: signal dynamics over time at different points within the colony (white star in the middle graphs). The green line marks the maximum activity, after which the signal decreases. Middle row: changes in the activity during colony growth. Bottom row: Raw speckle images.

The peak activity was initially observed at the centre of the colony. Over time, the activity "wave" migrated from the centre to the edges of the colony (Fig. 3.7). This behaviour of the signal was observed within all tested microbial colonies: *S. aureus*, *E. coli,* and *V. natriegens*.

3.7.2. Analysis of activity zones for different bacterial colonies in the time-space domain

The growth of a bacterial colony is affected by various conditions, so signals within the same "ring" are slightly different. It is necessary to do some averaging of all signals for a given radius so that each radius receives one signal that characterises it. Such averaging was performed by adopting the truncated average method [53], where the truncation was performed not in amplitude but at the time of the activity peak:

$$\overline{Env(D)} = \frac{1}{n-k_b-k_f}\left[Env(k_b+1)+,\ldots,+Env\left(L-k_f\right)\right], \qquad (3.8)$$

where L is the number of envelope signals at a given distance, $k_b$and k_f is the number of envelope signals that were truncated from each side. The obtained averaged signals were mapped as a function of distance from the centre and time (Fig. 3.8).

3.7.3. Spatial width of the activity zones

The signal width corresponds to the decrease from the peak value to a certain value. In real conditions, there should be a threshold at which the signal is still distinguishable against the noise. It is possible to find the width for each moment. This width will match the width of the "ring" at the corresponding time (Fig. 3.8).

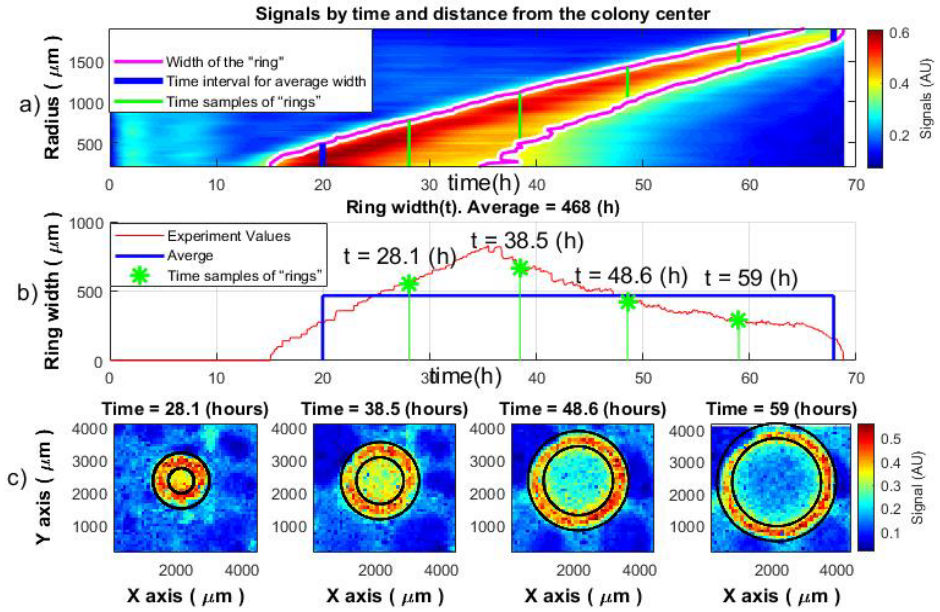

Fig. 3.8. Determination of the width of the activity "ring" for the colony of *S. aureus*: a) signal values and determined width of the activity ring (purple line); b) the obtained width of the activity "ring"; and c) comparison of the obtained width of the activity "ring" (black lines) for one colony at different times.

In Fig. 3.8 a) and b), it can be observed that although the change in the ring width is small, it can be considered constant with some deviations. The behaviour described for one selected colony was observed for all types of bacteria considered in this study. The width of the "ring" is different for each type of bacteria.

The Pirt study [54] provides a formula for calculating the width of the active zone or the "ring":

$$r = \frac{\omega\alpha}{2}t + r_0, \tag{3.9}$$

where ω is the width of the active cell proliferation zone of the colony, r is the colony radius at time t, and r_0 is the radius at $t = 0$; α is the specific growth rate also known as μ (h^{-1}), which can be found from the Gompertz equation (Eq. (3.6)). Thus, having the experimental data (the radius of the colony growth, the corresponding time, and μ), it is possible to calculate the width of the active zone or the width of the "ring" using Eq. (3.9).

3.8. Chapter conclusions

The microbial colony growth was not affected by laser illumination, and the behaviour of the growth curves obtained was highly similar to the behaviour of the ones from the cultivation under white light.

The proposed method, based on the analysis of laser speckle patterns using correlation subpixel analysis, provides an earlier response of growing bacteria in comparison with classical CFU growth detection under white light illumination. Accordingly, it is possible to shorten colony detection time by two or more times. Thus, speckle imaging offers unprecedented analytical opportunity for detecting CFU growth significantly earlier than visual inspection under white light.

The speckle imaging method with sensitive correlation subpixel analysis revealed that distinct activity zones within the colony exist, which migrate from the centre to the edges during the growth of the colony. A similar pattern of activity zone ("ring") migration in the colonies was observed in various microbial species. The migration speed of the "ring" varied across different microbial species reflecting their different growth rates typical for each of these species. This is a promising, powerful technology that has helped to visualize activity zones within the microbial colony. Previously, the presence of these zones was predicted mathematically.

The full version of the Thesis shows that while white light imaging clearly demonstrates colony presence, the subpixel correlation analysis method did not work under white light illumination. Neither colony growth nor ring effect was determined by subpixel correlation analysis under white light. These are the advantages of working with speckle images compared to white light.

4. LASER SPECKLE IMAGING FOR EARLY DETECTION OF ANTIBACTERIAL SUSCEPTIBILITY IN DISC DIFFUSION TESTS

Based on the posed aims and tasks, Chapter 4 of the doctoral Thesis describes the application of the proposed analysis method for early detection of antibacterial susceptibility in disc diffusion tests as a research object. The chapter covers experimental confirmation of the capabilities of earlier detection of bacterial reactions to antibiotics and analyses the mathematical model of the inhibition (or sterile) zone size changing.

4.1. Introduction to the chapter

Rapid identification of the pathogen and determination of its susceptibility to antibiotics can provide targeted pharmacological intervention at the early stages of the disease, increasing patient survival chances. The EUCAST-standardised phenotypic resistance tests, such as disk diffusion and E-test, require 16–24 hours to obtain results [55]. Therefore, new methods are needed to detect changes in microorganisms faster. The proposed technique of laser speckle imaging with correlation subpixel analysis allows for identifying dynamics and changes in the zone of inhibition, which is impossible to observe with classical methods and obtains the resulting zone of inhibition diameter earlier than the disk diffusion method, which is recommended by the European Committee on Antimicrobial Susceptibility Testing (EUCAST). These results could improve mathematical models of changes in the diameter of the zone of inhibition around the disc containing the antimicrobial agent.

4.2. Comparison of the results obtained with the laser speckle technique without and with the algorithm

This subsection compares the behaviour of the zone of inhibition for raw speckle images and for speckle images processed using subpixel correlation analysis. Consider bacteria that are susceptible to the antibiotic (Fig. 4.1).

The correlation subpixel algorithm allows for the detection of submicron bacterial events (e.g., the formation of a zone of inhibition) earlier than without the algorithm (Fig. 4.1). It can be observed that when executing the algorithm in the experiment, the zone of inhibition can be detected after 3.3 hours, and without it, the zone of inhibition can be detected no earlier than after 4.5 or more hours.

The intriguing outcome can be observed when the bacteria are completely resistant to the antibiotic, based on raw speckle images, and the zone of inhibition is not observed at all, while the subpixel correlation analysis demonstrates zone formation (demonstrated in the full version of the Thesis). This indicates that in some situations, the zone of inhibition may form even if it is not detected by the “naked eye” at all.

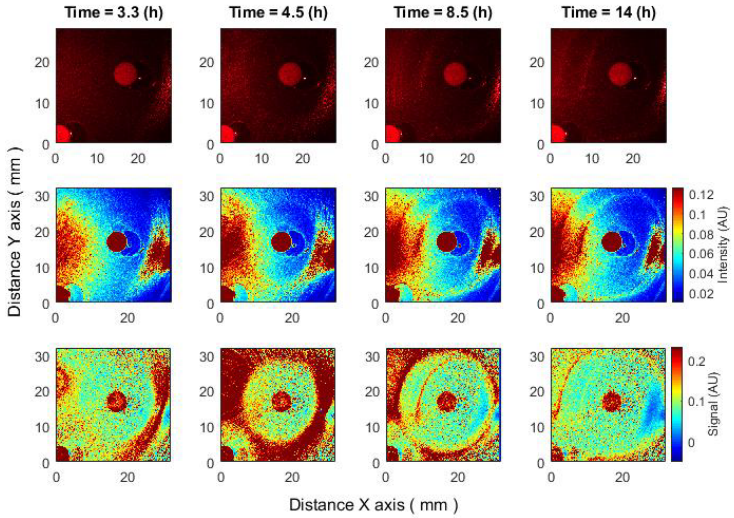

Fig. 4.1. Changes of the zone of inhibition as a function of time. Bacteria: *E. coli*, antibiotic CIP 5 µg. Recorded raw laser speckle images in time (top row), records processed by smoothing filter, contrast enhancements (middle row), and resulting images after the subpixel correlation analysis (bottom row).

4.3. Early detection of the formation of a zone of inhibition

A zone of inhibition appears "suddenly" 3–4 hours from the beginning of the experiment, immediately possessing a certain radius. New experiments were conducted to better understand these processes.

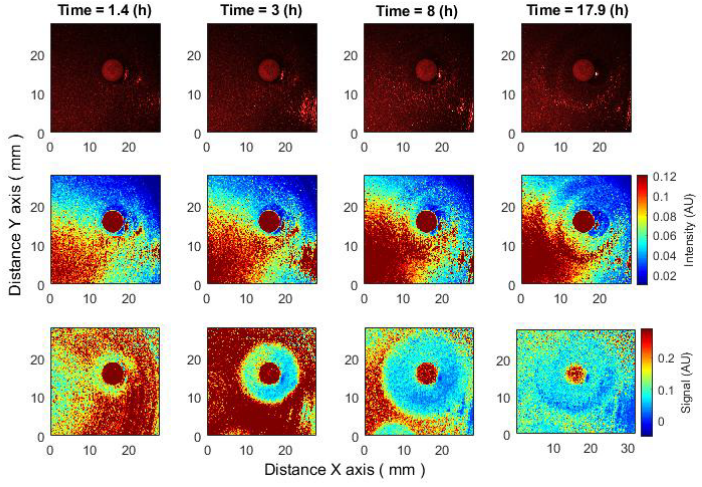

Fig. 4.2. Antibiotics are placed 4–4.5 hours after bacteria inoculation. The zone of inhibition changes as a function of time. Bacteria: *E. coli*, antibiotic CIP 5 µg. Recorded raw laser speckle images in time (top row), records processed by smoothing filter, contrast enhancements (middle row), and resulting images after the subpixel correlation analysis (bottom row).

The antibiotic discs were placed on the surface 4–4.5 hours after the bacteria inoculation (rather than immediately). Bacterial activity can be detected 3–4 hours after inoculation (Chapter 3). The zone of inhibition is noticeable only in contrast to the activity of bacteria; accordingly, it also cannot be visible until this moment. It is expected that the application of antibiotic discs 4–4.5 hours after bacterial inoculation would immediately allow the detection of the formation of the zone of inhibition.

This effect can be observed in a signal proportional to activity, i.e., after subpixel correlation analysis. When observing raw speckle images, this effect may not be noticeable since it is not the activity of bacteria observed there but their presence (Fig. 4.2).

4.4. Spatial-temporal analysis of changes of the zone of inhibition

The formation of a zone of inhibition is characterised by a decrease in activity. That is, looking for a drop after peaks of the signal envelope. To avoid the influence of noise, it is worth averaging the signal envelopes over each radius as it moves away from the centre (from the antibiotic) (Eq. (4.1)).

$$\overline{Env[r,n]} = \left[\frac{1}{M_{R1}}\sum_{m_{R1=1}}^{M_{R1}} Env_{m_{R1}}[n], \ldots, \frac{1}{M_{Rk}}\sum_{m_{Rk=1}}^{M_{Rk}} Env_{m_{Rk}}[n]\right], \quad (4.1)$$

where M_{Rk} is the number of envelope signals at a given distance/radius from the centre.

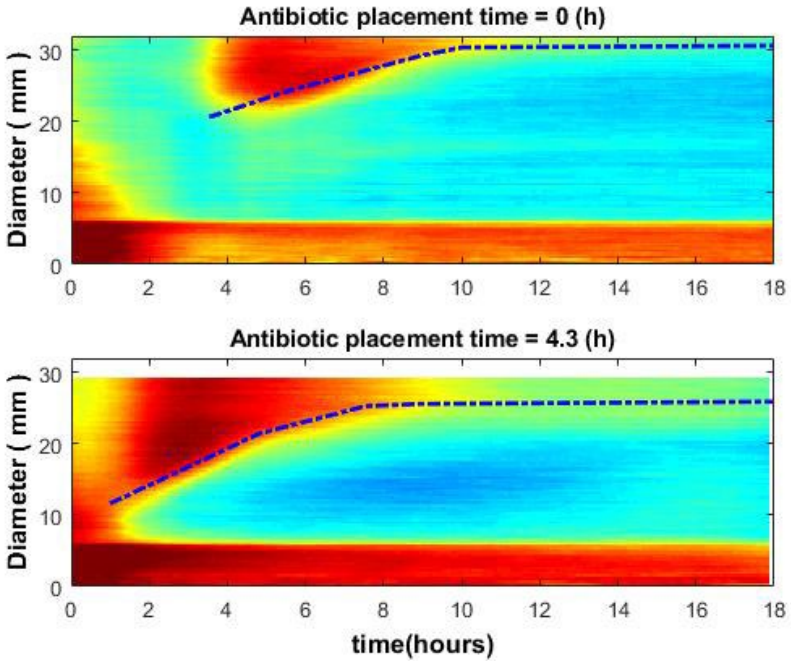

Fig. 4.3. The growth of *E. coli* around the Ciprofloxacin disc (5 µg). Spatial-temporal changes of the inhibition zone: 1) the antibiotic is placed immediately after the bacteria (top); 2) the antibiotic is placed 4.3 hours after the bacteria inoculation (bottom).

The beginning of the signal drop may indicate the appearance of a zone of inhibition in this place. In the situation where antibiotics are placed without bacteria, such behaviour was not found (Fig. 4.4).

By putting the averaged signal envelopes for all radii together, a spatio-temporal image can be obtained. Figure 4.3 (top) illustrates the case of bacteria susceptible to antibiotics. Antibiotics were placed on the Petri dish immediately after the bacteria inoculation. It can be observed that there is no space-time reaction before 3.5–4 hours. This is due to the reason described above – the activity of bacteria is not noticeable; accordingly, the zone of inhibition is not visible. Consider similar images when the antibiotic was placed on the Petri dish 4–4.5 hours after the bacteria inoculation (Fig. 4.3 (bottom)). Then there is no such "gap", and the spatio-temporal image is continuous.

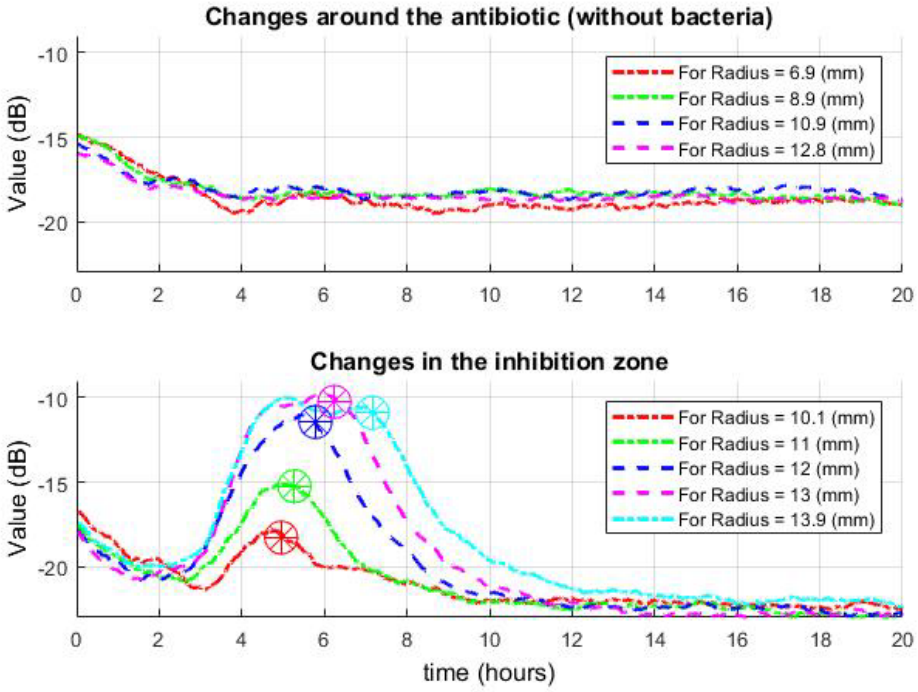

Fig. 4.4. Change of signals envelope over time for several different radii around the antibiotic: without bacteria (top row) and with bacteria (bottom row). In the bottom graph, it is observed that as it moves away from the centre, the drop (which means the appearance of a zone of inhibition in this place) occurs later (stars in a circle).

4.5. Mathematical model of the inhibition zone size changing

According to the study [56], the radius of the inhibition zone is demonstrated by Eq. (4.2).

$$r = \sqrt[2]{4D(\ln(c) - \ln(\mathrm{MIC})) \times t}\,, \tag{4.2}$$

where c is antibiotic concentration, MIC is the minimum inhibitory concentration, t is the time of antibiotic diffusion, and D is the diffusion coefficient received from Fick's second law of diffusion [57] (Eq. (4.3)).

$$\frac{\partial c(x,t)}{\partial t} = D\frac{\partial^2 c(x,t)}{\partial x^2}. \tag{4.3}$$

There are three unknowns in the model, MIC, D, c, and number 4, which can be replaced by one constant. Thus, a simple relationship is obtained between the radius of the zone of inhibition and time (Eq. (4.4)).

$$r = \sqrt[2]{\text{const} \times t}. \tag{4.4}$$

Having obtained the experimental curves, it is possible to choose the parameter of this constant that is closest to the model. Consider the same bacterium – *E. coli*, and the same antibiotic – Ciprofloxacin, but for two different cases: 1) the antibiotic is placed immediately after the bacteria; 2) the antibiotic is placed 4.3 hours after the bacteria (Fig. 4.3). The results are presented in Fig. 4.5.

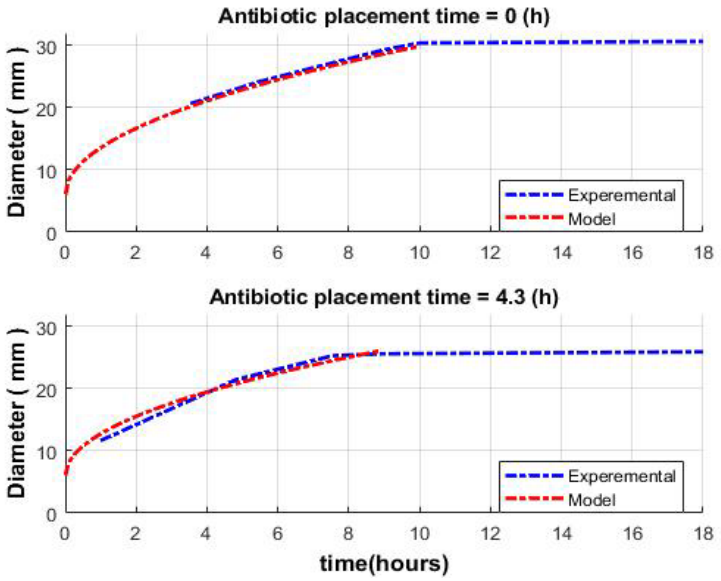

Fig. 4.5. Spatio-temporal curves for experimental data and model for *E. coli* around the Ciprofloxacin disc (5 μg).

For each sensitive bacterium, finding the set of parameters against each antibiotic is necessary. In the case of resistant bacteria, these curves might be unpredictable, and then approximations will not work.

4.6. Chapter conclusions

In this chapter, the clinically significant dynamics and changes of the zone of inhibition were evaluated by processing laser speckle images with correlation subpixel analysis. The zone of inhibition can be detected on the "signal presence" background only when the bacteria are already visible (after 3–4 hours). However, if the antibiotic is placed on the Petri dish 4–4.5 hours after the bacteria inoculation, the bacteria are in sufficient concentration to be visible almost immediately with the subpixel correlation method. While observing raw speckle images in this case, the zone of inhibition is not immediately visible, but after a delay of several hours

(approximately 5 hours). This shows that the established method allows the observation of small changes in activity that cannot be observed in the raw data.

Many broad-spectrum antibiotics are given at intervals of 6–8 hours. Future advancements in identification and antibiotic susceptibility testing (ID/AST) methods should focus on providing results within this time frame, enabling timely adjustments in antibiotic therapy to optimise patient care [58].

The accuracy of the proposed mathematical model of inhibition zone growth curves, as demonstrated in this chapter, is verified in comparison with experimentally obtained curves. For each sensitive bacterium, to determine the radius of the inhibition zone early, these curves will be different, and it is necessary to find the set of parameters for each bacterium against each antibiotic. However, this approximation will not work here for resistant bacteria. Accordingly, it is worth paying attention to other forecasting methods, such as those based on artificial intelligence.

5. APPLICATION OF AN ARTIFICIAL NEURAL NETWORK TO ANALYSE SPECKLE DATA TO CLASSIFY GROWING AND NON-GROWING COLONIES AND ZONES

Based on the stated aims and tasks, Chapter 5 of the Doctoral Thesis describes the use of artificial intelligence to analyse speckle data before and after the correlation subpixel analysis. This is done to classify between growing (active) colonies and non-active colonies, or between zones of active growth and inhibition around the antibiotic discs. The chapter covers experimental confirmation of the classification capabilities of the situations described above.

5.1. Introduction to the chapter

The present chapter substantiates the capability of laser speckle imaging to categorise colonies (or zones with microorganisms) as active or not, which is nonvisible under white light illumination. This analytical capability is instrumental for investigating the influence of chemical agents, such as antibiotics, on bacterial growth dynamics. Two types of laser speckle data are used: 1) without the utilisation of a subpixel correlation method, serving to identify the presence of bacteria, and 2) with a sensitive subpixel correlation algorithm, which ascertains the status of bacterial activity: growing or not. For classification purposes, artificial neural networks (ANNs) were utilised [59].

5.2. Tools for classification of growing / non-growing bacterial colonies

5.2.1. Colony analysis with laser speckle technique almost without additional processing

Consider a measurement of a bacterial colony over 100 hours using the first data type. Within the initial 45–50 hours, the colony exhibits active growth. Then growth arrest occurs, presumably owing to nutrient depletion. Examination of the colony's cross-sectional diameter as a function of time reveals specific growth dynamics (Fig. 5.1). Upon reaching a certain diameter, the colony ceases to grow. Despite the presence of bacteria throughout the occupied diameter, it is unclear whether they are in a state of growth or stasis.

The intensity levels at varying distances from the colony's centre (Fig. 5.1, bottom row) show an increment in intensity at distinct temporal intervals, contingent on the distance from the centre. Once a specific intensity level is reached, it remains relatively constant. This information, however, does not furnish sufficient evidence to deduce the ongoing biological activities within the colony.

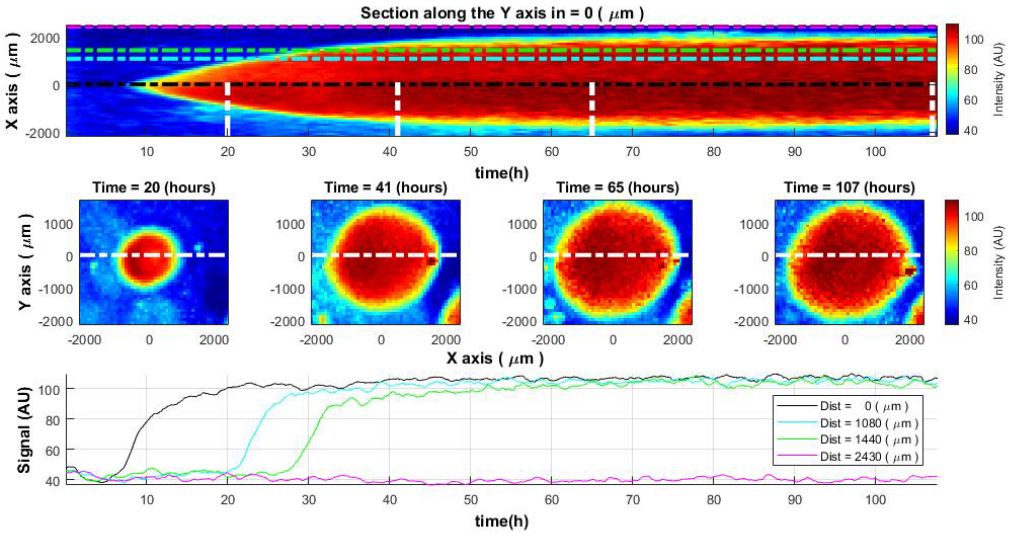

Fig. 5.1. Spatiotemporal distribution of the laser speckle reflectance intensity across the *V. natriegens* colony. The change of colony cross-sectional intensity over time (top) and colony size at specific time moments (middle row). The white lines in the top image define the time of the cross-section demonstration in the middle row images. Lines of different colours in the top and bottom images indicate the measurement of intensity level at the centre of the colony and at different distances from the colony centre (bottom).

5.2.2. Laser speckle technique with subpixel correlation analysis reveals growth changes within the colony

Alterations in the growth dynamics within a bacterial colony can be discerned using laser speckle imaging techniques with correlation subpixel analysis (the second algorithm). Observations indicate that once a specific diameter is attained, growth arrests. The signal indicative of bacterial activity begins to attenuate and vanishes (Fig. 5.2, top and middle rows). It becomes clear that the colony's growth has ceased.

Examining signal curves along the temporal axis at various distances from the centre of the colony (Fig. 5.2, bottom), one notes that bacterial growth (manifested as high signal values) migrates outward from the centre. At first, the strongest signal is observed at the centre and diminishes as the distance from the centre increases. Over time, the signal diminishes and vanishes approximately 45–50 hours into the initiation of the experiment, corresponding to the cessation of bacterial growth within the colony.

The observed behaviour was consistent across different experiments and bacterial species, such as *E. coli* and *S. aureus*.

In the full version of the Thesis, to detect the overall trend and reduce the influence of noise, the median of the signal envelope is calculated for each radius around the entire colony. This procedure allows you to observe the behaviour of the “overall” signal as a function of time and distance.

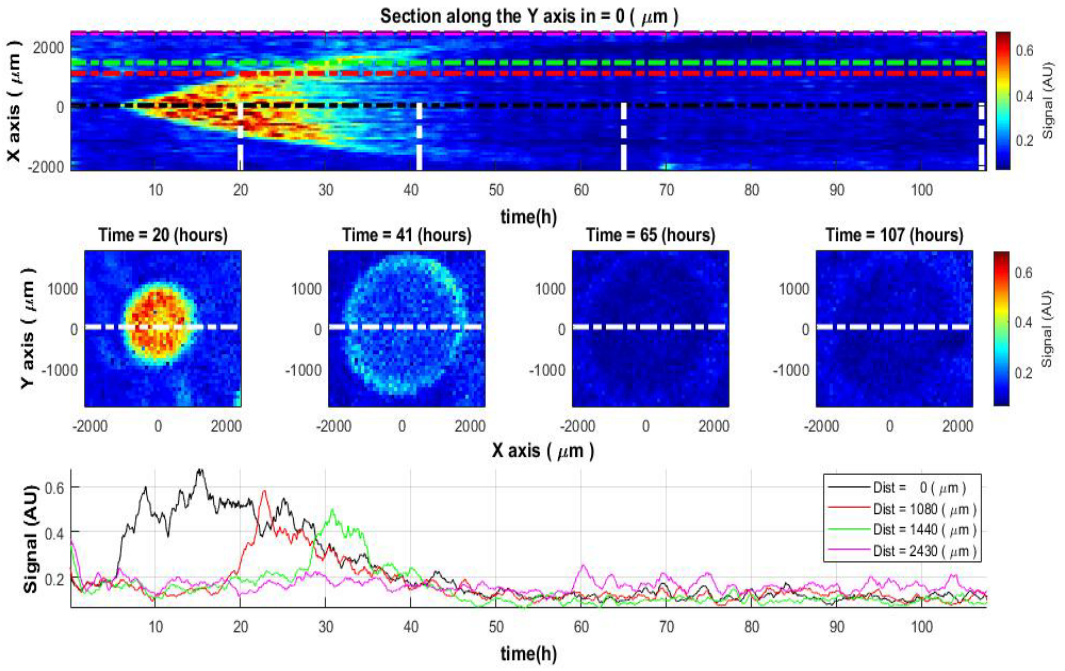

Fig. 5.2. Spatiotemporal distribution of the activity signal across the *V. natriegens* colony. The change of colony cross-sectional activity signal over time (top) and colony activity signal at specific time moments (middle row). The white lines in the top image define the time of the cross-section demonstration in the central images. Lines of different colours in the top and bottom images indicate the measurement signals at the colony's centre and at different distances from the colony centre (bottom).

5.2.3. Automatic classification between growing and non-growing bacterial colonies using artificial neural network

The current subsection demonstrates the ability to classify between active and inactive bacterial colonies based on the features described in the previous subsections (Fig. 5.3). The training set is 10 different colonies spanning three bacterial species. The duration of growth in these training experiments ranges from 25 to 68 hours. The test set is *V. natriegens* colonies with a longer observation period of 107 hours. Signals are divided into 3-hour sections. Two types of data (described above) were used. The aggregate data encompass thousands of signals for each colony in the training and test sets. A multilayer perceptron (MLP) was used.

This methodology could have broader applications in both research and practical fields, such as monitoring bacterial resistance to antibiotics or assessing the efficacy of novel antimicrobial compounds.

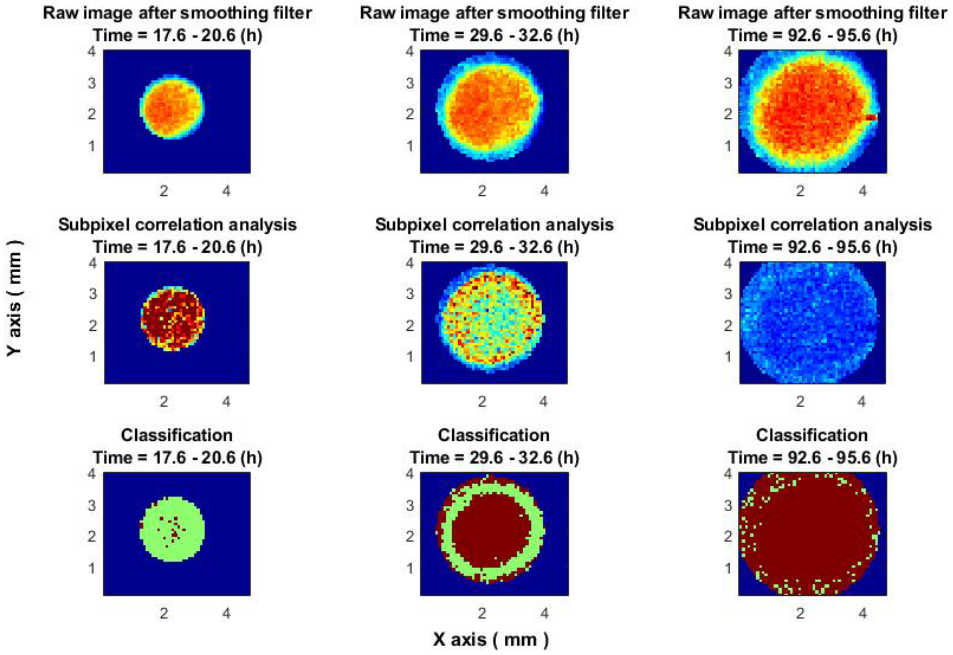

Fig. 5.3. Classifier performance at different times. The images in the top row are raw images of the colony after a smoothing filter. Central images – subpixel correlation analysis. Images in the bottom – classification result. In all images, the blue colour represents the out-of-colony region. In the bottom images (classification results), the results of non-growing zones are in brown, and the results of growing zones are in green.

5.3. Classifying between inhibition and active bacteria growth zones around the antibiotic discs using a neural network

5.3.1. The signal behaviour tendency at different radii from the antibiotic disc

As already described in Chapter 4, after placing the antibiotic on this medium with bacteria, the antibiotic begins to create around itself an inhibition zone, which has an almost circular shape and grows over time.

Consider the behaviour of the first type of data (Fig. 5.4). The formation of an inhibition zone is characterised by a stop of growth. At the time when the antibiotic influence reaches the measured area, the data value stops increasing. Thus, the closer the distance to the antibiotic 1) the cessation of growth in data values will occur earlier, and 2) the achieved value will be lower than values at the far distance. That is, the shape of the signals at the same radius from the antibiotic should be similar. Taken into account that these values are below the values outside the inhibition zone and, accordingly, more sensitive to the influence of noise, it is worth making a median of data over each radius as it moves away from the center (from the antibiotic) [47], [53], [60], (Eq. (5.1)).

$$\overline{Env[r,n]} = \left[median_{\{over\ m_{r1}\}}\left(Env[m_{r1},n]\right),\ldots,median_{\{over\ m_{rk}\}}\left(Env[m_{rk},n]\right)\right], \quad (5.1)$$

where m_{rk} is the number of envelope signals at a given distance/radius (k) from the centre.

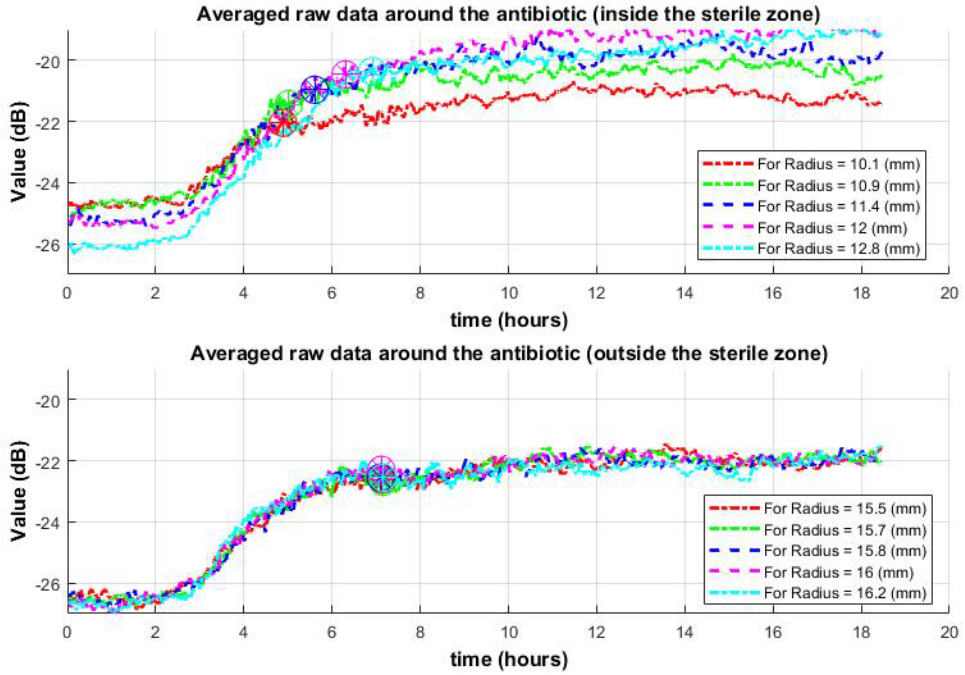

Fig. 5.4. Behaviour of median by radius data of the first type over time for several different radii around the antibiotic. On top, in the inhibition zone. At the bottom, out of the inhibition zone (with active bacteria). In the top graph, it is observed that as it moves away from the centre, the cessation of data value growth (which means the appearance of an inhibition zone in this place) occurs later. Outside the inhibition zone (bottom graph), the cessation of value growth occurs much later and simultaneously for different radii. The cessation of data values growth is indicated by circles.

Consider the second type of data. The inhibition zone is characterised by a decrease in activity after peak values of signals. For a demonstration of the signal's behaviour, like in the previous example, it is to make a median of signal envelopes over each radius (Eq. (5.1)). As it moves away from the antibiotic, the drop time will be later. The signals for radii outside the inhibition zone will be very similar to each other. The drop will occur later and almost simultaneously, supposedly due to the depletion of nutrients (Fig. 5.5).

Thus, both data types demonstrate an unconditional difference between the signals inside and outside the inhibition zone. However, the correlation subpixel signal better allows for distinguishing zones.

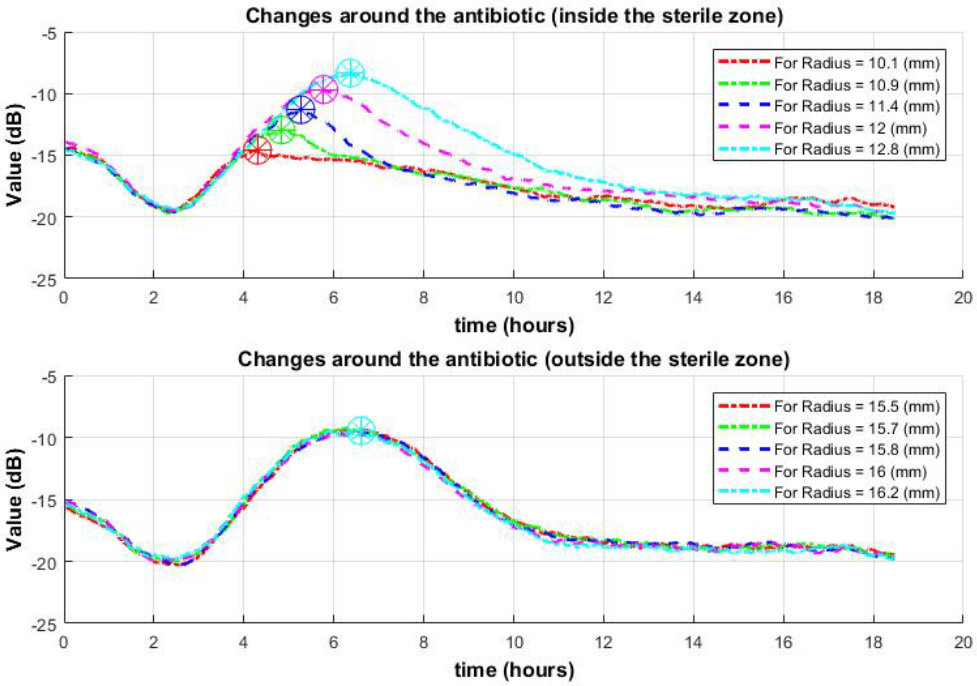

Fig. 5.5. Change of median by radius data of the second type over time for several different radii around the antibiotic. On top, in the inhibition zone. At the bottom, out of the inhibition zone (with active bacteria). In the top graph, it is observed that as it moves away from the centre, the drop (which means the appearance of an inhibition zone in this place) occurs later. Outside the inhibition zone (bottom graph), the signal falls much later and simultaneously for different radii. In this case, the drop is not due to antibiotics but to other reasons (for example, nutrient depletion).

5.3.2. Neural network for classification

The main goal of using a neural network in this subsection is to classify between 2 classes: 1) zones of active bacterial growth and 2) inhibition zones.

The full version of the Thesis describes considerations for designing a neural network [61]–[63]. Based on these considerations, the network parameters are as follows. The network is multilayer perceptron [59]: 1) two hidden layers (the first hidden layer is 30 neurons, the second hidden layer is 20 neurons, and the output layer is two neurons, according to the number of classes: bacteria or an inhibition zone); 2) learning rate = 0.03; 3) momentum = 0.5; and 4) epochs = 200.

To train the neural network, eight experiments with *E. coli* bacteria were conducted. Each such experiment involved an almost entire Petri dish where two antibiotics were placed, around which inhibition zones were formed. Each experiment had approximately 80–100 thousand signals of one type and the same number of signals of the second type of length T (15–18 h). The signals were divided into time windows of 1 hour to obtain a classification result during this short period of time.

5.3.3. Results

This subsection describes two methods to improve classification results by using knowledge about the antibiotic position and the growth process of the inhibition zone, using signal processing.

5.3.3.1. Improving classification results by class changing function as distance from antibiotic

Taking into account 1) that inhibition zones occur around the antibiotic, and antibiotic location and size are known, 2) that the inhibition zone grows in a shape close to a circle, the classification result can be improved. For this aim, the median of the class values obtained over each radius as it moves away from the antibiotic to the edges for each time window of 1 hour is calculated. The class characterising the inhibition zone can be designated as Class 1, and the class characterising the area with bacteria can be designated as Class 2. At a radius close to the antibiotic, the median of the class result will be close to 1 (since this is an inhibition zone). At a radius far from the antibiotic, the median of the class result will be close to 2 (since this is an area with active bacteria). The distance of switching from Class 1 to Class 2 will correspond to the radius of the inhibition zone for each considered time window (Eq. (5.2)).

$$\langle Class(r) \rangle = [median\,(Class[m_{r1}]), \ldots, median(Class[m_{rk}])], \tag{5.2}$$

where m_{rk} is the number of class points per radius k from the centre.

Figure 5.6 (middle and bottom row) shows the class change as a function of radius around two antibiotic discs and improving classification results for one selected time window.

Such an improvement can reach 5–20 percent.

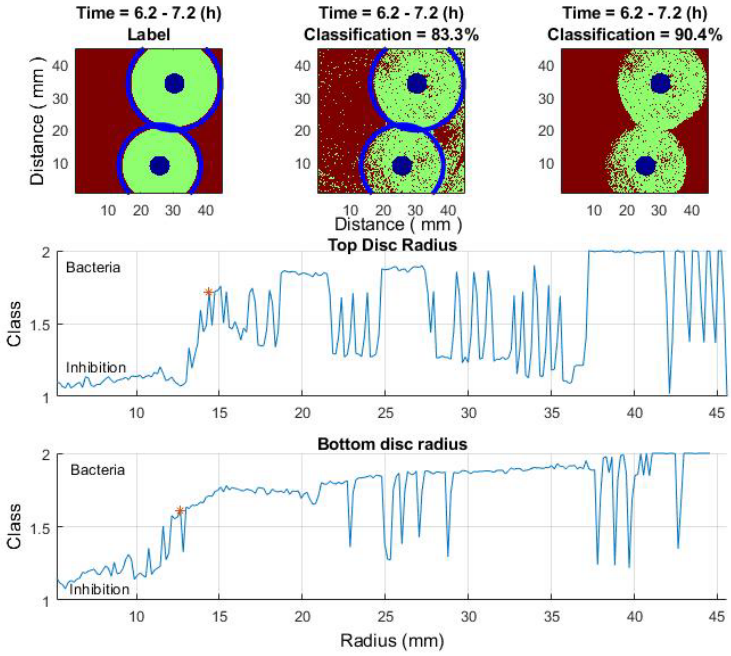

Fig. 5.6. Improving classification results. Time window 6.2–7.2 h. Top row: 1) left image – labelling; 2) central image – classification result; 3) right image – classification result after the class estimation algorithm. The middle row – class change as a function of radius (top antibiotic disc). Bottom row – class change as a function of radius (bottom antibiotic disc).

5.3.3.2. Improving classification results using radius-averaged signals

Another approach to improve the classification result uses the same two factors (Subsection 5.3.3.1). Thus, it is possible to make a median of the signals over the radius around the antibiotic. Instead of many signals, for each radius, there will be only one median signal from the correlation subpixel method and one from the average by an N × N pixel window. The median signal preserves the trend of the signals, but the noise is suppressed [47], [53], [60], which improves the classifier's performance. Also, replacing many signals with a small number of median signals will reduce the operating time of the classifier. This approach makes it possible to achieve higher classification performance (Fig. 5.7).

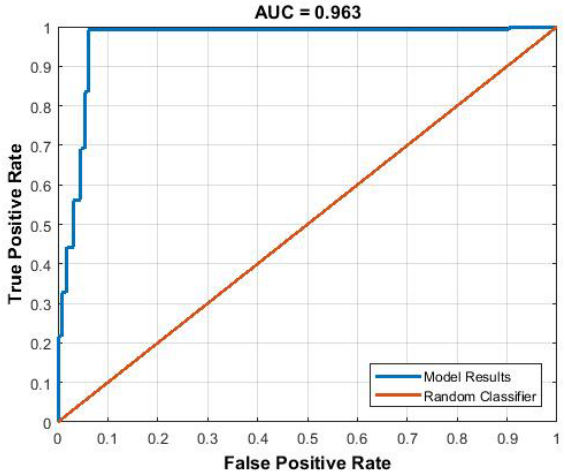

Fig. 5.7. ROC curve of classification using a median signal.

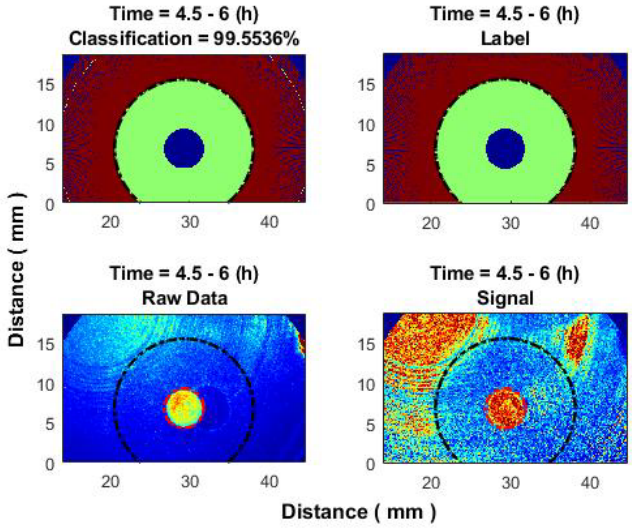

Fig. 5.8. Improving classification results by one median signal over each radius. Time window: 4.5–6 h. Top left – classification result; top right – labels; bottom left – average over N × N pixel window; bottom right – correlation subpixel algorithm.

However, if a classification error occurs, an incorrect result will be obtained not at one point in space but along an entire specific radius (in the “ring” shape) (Fig. 5.8). If a “ring” is located deep in another class, then it can be easily detected and removed using additional algorithmic tools. If it is located at the transition point from one class to another, then it is more difficult to detect the error.

5.4. Chapter conclusions

The laser speckle imaging with correlation subpixel algorithm allows the detection of subtle changes in the object under observation, effectively distinguishing colonies where bacteria are still proliferating colonies (or zones) from dormant or dead colonies (or zones), which is not achievable with laser speckle without correlation subpixels algorithm or white-light imaging alone.

In the inhibition zone, the decrease in the signals' value occurred in a dynamic manner (as one moves away from the antibiotic, this occurs later), representing the radius of the inhibition zone. Outside the inhibition zone, the signal decreased much later and simultaneously for different radii. The signals in both zones definitely differed from each other. Using the proposed methods, such as 1) finding the radius at which the inhibition zone ends, the correct classification increases by 5–20 percent, reaching 83–92.5 percent (see the full version of the Thesis); 2) median signal per radius, the correct classification increases even more, reaching over 96 percent (up to 99 percent).

Thus, by understanding the specificity of signals using an algorithmically appropriate base, high classification can be achieved.

The method could become instrumental in various research domains, from studying bacterial growth dynamics to evaluating the efficacy of antimicrobial substances.

6. COMPARISON OF THE PROPOSED METHOD WITH OTHER METHODS BASED ON THE USE OF LASER SPECKLE TECHNIQUES

Based on the stated aims and tasks, Chapter 6 of the Doctoral Thesis performs a comparison of proposed algorithms in the literature for the microorganisms' behaviour monitoring, as described in this study, correlation subpixels algorithm as a research object.

6.1. Algorithms of microorganisms' behaviour analysis proposed in the literature

6.1.1. Spatial contrast analysis

To prove that the laser speckle imaging technique is a reliable method for monitoring microbial concentration, the literature suggests analysing such parameters as the spatial contrast [64] (Chapter 1, Eq. (1.11)) and the speckle grain size [19]. This is because, as the concentration of scatterers in the sample increases, the dynamics of Brownian motion also increase. Consequently, the spatial contrast decreases. The spatial contrast of the speckle image can provide information about the nature of the medium, for example, its viscosity [65] or the number of diffusers [66]. The image's contrast can also detect the dynamics in the medium due to the variation of the speckle grains. When microorganisms move on the observed surface, the speckle pattern becomes blurred and the speckle contrast is reduced. Thus, lower contrast values correspond to more intense dynamic changes in the observed medium.

6.1.2. Speckle size analysis

The speckle grain size is a parameter affected by the number or the size of the scatterers in the medium. The average speckle size may be estimated by the FWHM of the autocovariance function (Chapter 1, Eq. (1.10)). Thus, speckle size can be calculated from the speckle image, which is useful for measuring the roughness of a surface. The study [23] uses this assay to analyse bacterial growth in liquid culture media. It was found that speckle grain size decreases with bacterial growth. However, since the current study works on the surface, on the solid (agar) media, the results may differ, and this needs to be verified.

6.1.3. Decorrelation time analysis

Another useful approach to using the laser speckle technique to determine a microorganism's activity is to measure the time or rate of decorrelation [38] (Chapter 1, Eq. (1.12)). The decreases in the temporal correlation value are proportional to the microorganisms' concentration and activity.

6.1.4. Temporal contrast analysis

Along with the spatial contrast method, several studies for the characterisation of the activity of a dynamic speckle pattern suggest using the temporal contrast method [6] or other methods based on the difference between time frames. These methods can provide certain benefits compared to spatial contrast analysis and highlight the hidden effects discovered in this

work using the correlation subpixels algorithm. Using temporal contrast instead of spatial contrast allows operation with higher spatial resolution, however, at the expense of temporal resolution. If temporal samples are statistically independent, then temporal contrast analysis provides high results when estimated from 15 or more speckle frames [53].

6.2. Comparison of algorithms

6.2.1. Spatial contrast analysis

The calculation of spatial contrast was tested in experiments with bacteria and fungi on solid (agar) media. The ability to obtain the “ring of activity” effect, which characterises the growth of a colony, was tested as described in Chapter 3. Fig. 6.1 demonstrates the result of the comparison by the algorithm. The contrast demonstrates the presence of a colony but does not reveal the "ring effect" that is noticeable using the correlation subpixel algorithm.

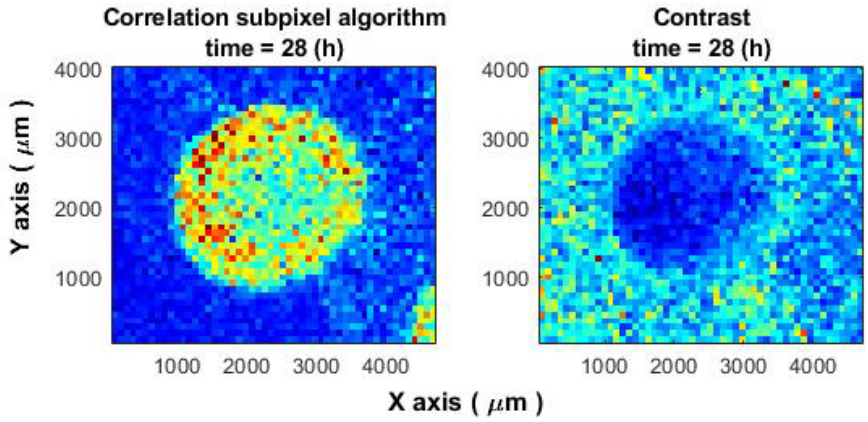

Fig. 6.1. Comparison of the correlation subpixel algorithm with spatial contrast analysis. The bacterial colony of *Vibrio natriegens.* The contrast analysis does not reveal the “ring effect”.

6.2.2. Decorrelation time analysis

To analyse the decorrelation method, experiments with bacteria and fungi were conducted. Figure 6.2 shows the change in the normalised cross-correlation value over time between the 1st frame and subsequent frames in two cases: with and without microorganisms. This method enables the detection of the presence of microorganisms but does not reveal hidden effects within colonies**.**

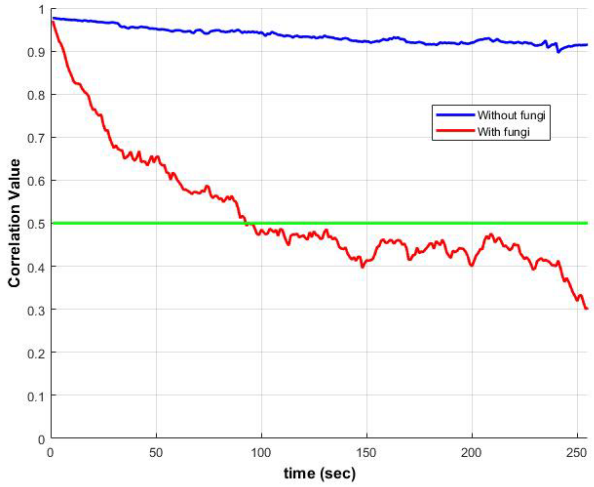

Fig. 6.2. Change in the value of the normalised cross-correlation over time between the first frame and subsequent frames in two cases: 1) without microorganisms (blue) and 2) with microorganisms (red).

6.2.3. Speckle size analysis

Speckle size measurements in experiments with bacteria and with fungi on solid (agar) media before and after the appearance of microorganisms in the observation area were carried out several times and with different cultures.

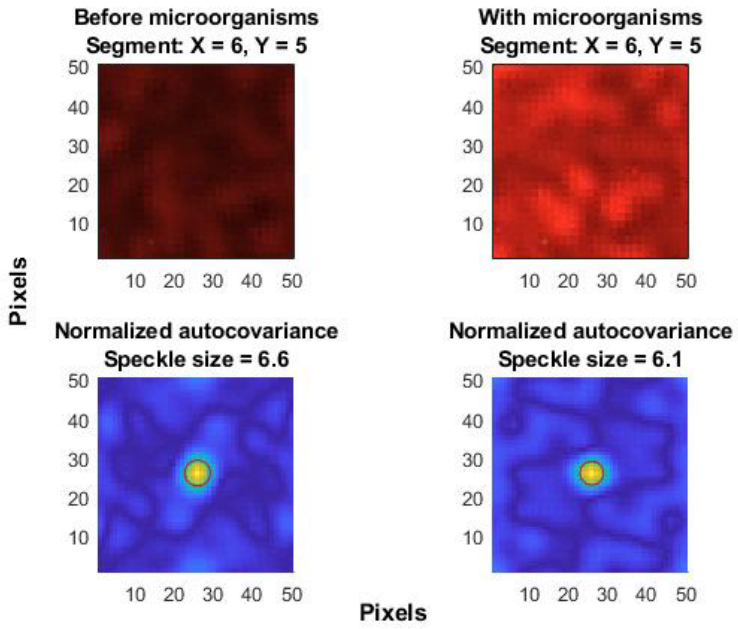

Fig. 6.3. Analysis of microorganism behaviour by speckle size calculation. For one spatial window.

This is demonstrated using the example of *Candida albicans* fungi. The experimental field was divided into M × M pixels, and the speckle size was measured for each such window (Fig. 6.3). In the full version of the Thesis, a statistical analysis is carried out to confirm this result across the entire calculated field. The algorithm demonstrated the following result: the speckle size remains almost unchanged (measured changes can be attributed to statistical errors).

6.2.4. Temporal contrast analysis

It is expected that methods based on the difference between time, along with the subpixel correlation algorithm, can also detect hidden effects on the growth, behaviour, and inhibition of microorganisms. Figure 6.4 shows a comparison of a part of a *V. Natriegens* bacterial colony processed by two methods: the subpixel correlation algorithm and the temporal contrast method. In both cases, the ring effect is visible. As described in Subsection 6.1.4, the spatial resolution of the temporal contrast method is better than that of the subpixel correlation algorithm.

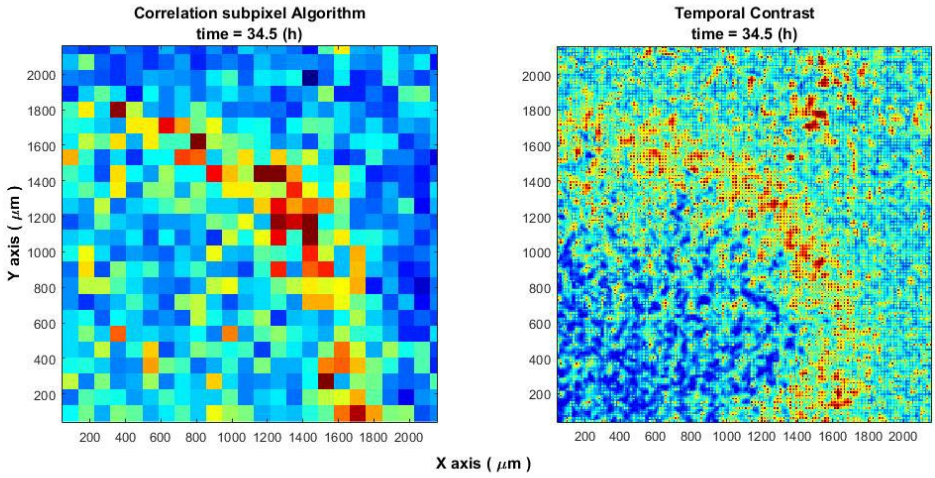

Fig. 6.4. Edge of a bacterial colony. On the left – the correlation subpixel analysis. On the right – the temporal contrast analysis. Both methods detect the "ring effect" described in Chapter 4.

However, a time analysis will also be carried out. To demonstrate the behaviour of a signal, it is worth using not recordings of microorganisms but a deterministic signal with clearly known changes in the time and frequency domains. For this purpose, a linear sweep was chosen. Signal parameters: linear sweep, frequency increase between 5–185 mHz during 2500 s, $Fs = 400$ mHz. Since a time window is used to calculate temporal contrast or similar algorithms, this has been taken into account: The averaging of frames was performed in the signal, every N sample. Although in Subsection 6.1.4 it is written that N is longer than 15, for greater graphical clarity, a smaller number is used: $N = 4$. Figure 6.5 demonstrates that in this case, temporal frequencies higher than Fs/N will "curl up" into the area of lower frequencies.

That is, the effect of temporary aliasing is observed. The full version of the Thesis demonstrates the result of the simulation with speckle images, confirming this problem.

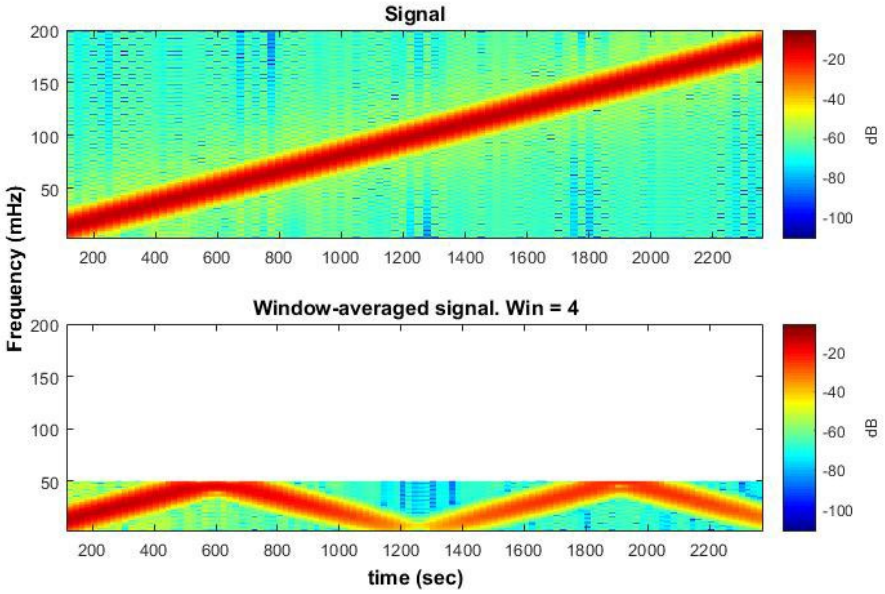

Fig. 6.5. Spectrogram of linear sweep signal. Top image – the sampling frequency satisfies the Nyquist criterion. Bottom image – the same signal but averaged over the time window $N = 4$. In this case, the effect of temporal aliasing is observed.

6.3. Chapter conclusions

In this chapter, the widely described in the literature algorithms for analysing speckle data of microorganism behaviour were considered and compared with the proposed method – correlation subpixel analysis.

The spatial contrast analysis detects a growing bacterial colony but cannot detect migration of activity within the colony, which is detected using subpixel correlation analysis.

The decorrelation method detects microorganisms' presence but does not reveal hidden effects within colonies (the “ring effect”).

Speckle size measurements in experiments with bacteria and fungi on solid (agar) media did not reveal significant changes in this parameter. Accordingly, for these conditions, it is worthwhile to resort to other methods.

Methods based on the difference between time frames, such as the temporal contrast method, can detect hidden effects. This can be achieved with high spatial resolution, but the undesirable effect is a decrease in temporal resolution. Lowering the temporal resolution will require a higher frame rate. Failure to take this aspect into account will lead to the effect of temporary aliasing. The challenge of temporal aliasing in such methods is a topic for future research. Unlike the methods described in this chapter, the proposed correlation subpixels algorithm, in addition to spatial analysis, converts a speckle image sequence into a time signal

array. An important advantage of this approach is that signal processing algorithms can be applied to the obtained signals.

The results obtained in the current chapter demonstrate the advantages of the proposed method – correlation subpixel analysis.

RESULTS AND CONCLUSIONS

The goal of the Thesis was to develop a novel approach for non-contact detection and assessment of submicron activity or growth of submicron objects over a large area, as well as the ability to classify and evaluate specific submicron objects or events. One of the challenges was the approach to signal processing, for which a correlation subpixel algorithm was implemented to convert a sequence of video images into signal arrays. Another challenge stemmed from the fact that changes in the growth and inhibition of microorganisms manifest as very low-frequency signals (mHz). Technologies designed for processing such low-frequency signals typically require complex equipment and are suited for observing "global-scale" processes. Therefore, it was essential to develop compact, small-scale equipment capable of operating within this frequency range and processing these signals. The developed approach holds potential for application in other areas that require the processing of very low-frequency signals, which could stimulate further research in this field. The proposed method demonstrated sensitivity to hidden effects that were either undetectable by other approaches or would have required significantly higher frame rates for detection. Additionally, it was shown to perform effectively in noisy environments. The use of artificial neural networks to analyse signals obtained from the sequence of images (processed using the proposed algorithm), along with additional post-processing based on an understanding of the signal properties, resulted in significant improvements in the classification of active (growing) and inactive zones – an outcome not achievable with raw speckle data alone.

The goal of the Thesis was effectively achieved, and in the process, the following steps were completed, giving the following results:

- An analytical study of similar research and studies revealed the most popular and accurate approaches and methods in this field:
  - analysis of speckle contrast;
  - analysis of speckle size;
  - analysis of decorrelation time or rate of speckle images.
- There is a relationship between all the studied approaches with correlation analysis. Thus, it becomes clear that correlation analysis is an important, powerful, and promising tool for analysing speckle patterns (including the medical/biological field).
- Correlation analysis methods of speckle images described in the literature for detecting mechanical vibrations and reconstructing audio signals were studied. The conclusions drawn were used. However, due to the distinctive features of signals characteristic of microorganism behaviour, the algorithm was modified. Methods for fast and, at the same time, accurate implementation of the algorithm were considered, and the most suitable one was proposed.
- An approach that allows monitoring of the dynamics of submicron events, highlighting hidden effects, was developed for medical and microbiological needs in the analysis of the behaviour of microorganisms.

All developed methods and algorithms were experimentally analysed to test the hypotheses defined for this study:

- The first hypothesis was validated through experiments designed to observe colony growth using two distinct illumination methods: 1) white light illumination, and 2) the laser speckle technique, followed by subsequent analysis. Analysis of laser speckle patterns using a subpixel correlation algorithm enabled earlier detection of bacterial growth compared to the conventional colony-forming unit (CFU) method under white light illumination.
- The second hypothesis was validated through experiments observing colony growth using the laser speckle technique under two approaches: 1) without additional analysis, and 2) with correlation subpixel algorithm analysis. The proposed correlation subpixel analysis revealed the presence of a distinct activity zone within the colony, which migrates from the centre to the edges during growth.
- The third hypothesis was validated through the execution and analysis of experiments observing colony growth in a highly noisy environment using two approaches: 1) the laser speckle technique without additional analysis, and 2) the laser speckle technique with correlation subpixel algorithm analysis. The proposed correlation subpixel algorithm successfully detected the presence of a colony, whereas the laser speckle technique, without additional analysis, failed to do so.
- The fourth hypothesis was validated through the analysis of experimental data involving both bacterial colonies and zones of inhibition around antibiotic disks using two approaches: 1) the laser speckle technique without additional analysis, and 2) the laser speckle technique with correlation subpixel algorithm analysis. Although the laser speckle technique without additional analysis enables the visualisation and detection of colonies and zones of inhibition, the laser speckle technique with correlation subpixel algorithm exhibits enhanced sensitivity to subtle changes, allowing for reliable differentiation between various data types. This capability was further confirmed through the implementation of a classifier.

All theoretical questions posed in this study were experimentally validated through the proposed and developed approaches and methods. As a result, a non-invasive, non-contact method was introduced within the scope of this Thesis, enabling earlier detection of bacterial growth compared to conventional colony-forming unit (CFU) detection under white light illumination. This method allows for the visualisation of previously undetectable, hidden activity zones within microbial colonies and facilitates the identification of dynamic changes in the zone of inhibition around antibiotic disks, which would otherwise remain undetected. Consequently, classifiers developed based on this method accurately distinguished between active and inactive zones. Future research may focus on developing simulation models and forecasts of microorganism colony growth and inhibition zone dynamics.

BIBLIOGRAPHY

[1] Rigden, J. D., Gordon, E. I. "Granularity of scattered optical maser light." Proceedings of the Institute of Radio Engineers, 50(11), 2367, (1962).
[2] Oliver, B. M. "Sparkling spots and random diffraction." Proceedings of the IEEE, 51(1), 220–221, (1963).
[3] Fujii, H., and T. Asakura. "Effect of surface roughness on the statistical distribution of image speckle intensity." Optics communications 11.1, pp. 35–38, (1974).
[4] Hamed, A. M., Saudy, M. "Computation of surface roughness using optical correlation." Pramana 68, pp. 831–842, (2007).
[5] Heikkinen, J., Schajer, G. S. "Remote surface motion measurements using defocused speckle imaging." Optics and Lasers in Engineering, 130, 106091, (2020).
[6] Boas, D. A., Dunn, A. K. "Laser speckle contrast imaging in biomedical optics," J. Biomed. Opt., vol. 15, no. 1, p. 11109, (2010).
[7] Hahn, F., Hernández, G., Echeverría, E., Romanchick, E. "Escherichia coli detection using thermal images," Canadian Biosystems Engineering, vol. 48 (4), 7–13, (2006).
[8] Volpe, P. L. O. "Flow microcalorimetric measurements of the antibacterial activity of the homologous series m-alkoxyphenols and p-hydroxybenzoates on Escherichia coli," J. Braz. Chem. Soc., vol. 8, no.4 (1997).
[9] Skarstad, K., Steen, H. B., Boye, E. "Cell cycle parame-ters of slowly growing Escherichia coli B/r studied by flow cytometry," J. Bacteriol. 154 (2), 656–62, (1983).
[10] Tan, W., Oldenburg, A. L., Norman, J. J., Desai, T. A., Boppart, S. A. "Optical coherence tomography of cell dynamics in three dimensional tissue models," Opt. Exp. 14, 7159–7171, (2006).
[11] Goodman, J. W. "Speckle Phenomena in Optics. Theory and Application", Chapter 8, Roberts and Company, Englewood, Colorado, (2007).
[12] Goodman, J. W. "Introduction to Fourier Optics", 3rd ed., Roberts, (2005).
[13] Federico, A., Kaufmann, G. H., Galizzi, G. E., Rabal, H., Trivi, M., Arizaga, R. "Simulation of dynamic speckle sequences and its application to the analysis of transient processes," Opt. Commun. 260, 493–499, (2006).
[14] Duncan, D. D., Kirkpatrick, S. J. "The copula: a tool for simulating speckle dynamics", Journal of Optical Society of America, A, 25(1), 231–237, (2008).
[15] Duncan, D. D., Kirkpatrick, S. J. "Algorithms for simulation of speckle (laser and otherwise)," Biomedical Optics (Optical Society of America), V, 6855, p. 685505, (2008).
[16] Oulamara, A., Tribillon, G., Duvernoy, J. "Biological activity measurement on botanical specimen surfaces using a temporal decorrelation effect of laser speckle," J. Mod. Opt. 36, 165–179, (1989).
[17] Lehmann, P. "Surface-roughness measurement based on the intensity correlation function of scattered light under speckle-pattern illumination," Appl. Opt. 38, 1144–1152, (1999).
[18] Ennos, A. "Speckle interferometry," in Laser Speckle and Related Phenomena, J. C. Dainty, ed. (Springer-Verlag, 1975).
[19] Piederriere, Y., Cariou, J., Guern, Y, Le Jeune, B., Le Brun, G., Lotrian, J., Scattering through fluids: speckle size measurement and Monte Carlo simulations close to and into the multiple scattering, Optics Express 12, 176–188, (2004).
[20] Goodman, J. W. Statistical Optics (Wiley, 1985).

[21] Duncan, D. D., Kirkpatrick, S. J. “Can laser speckle flowmetry be made a quantitative tool?” J. Opt. Soc. Am. A. Opt. Image Sci. Vis., vol. 25, no. 8, pp. 2088–2094, (2008).
[22] Briers, J. D., Webster, S. “Laser speckle contrast analysis (LASCA): A nonscanning, full-field technique for monitoring capillary blood flow,” J. Biomed. Opt., vol. 1, no. 2, 174–179, (1996).
[23] Zdunek, A., Muravsky, L. I., Frankevych, L., Konstankiewicz, K. "New nondestructive method based on spatial-temporal speckle correlation technique for evaluation of apples quality during shelf-life", International Agrophysics, 21(3), 305–310, (2007).
[24] Nader, C. A., Pellen, F., Loutfi, H., Mansour, R., Jeune, B. L., Brun, G. L., Abboud, M., "Early diagnosis of teeth erosion using polarized laser speckle imaging.", Journal of biomedical optics, 21(7), 071103–071103, (2016).
[25] Fercher, A. F., Briers, J. D., “Flow visualization by means of single-exposure speckle photography”, Opt. Commun. 37, 326–330, (1981), https://doi.org/10.1016/0030-4018(81)90428-4
[26] Peters, W. H., Ranson, W. F. “Digital image techniques in experimental stress analysis,” Optical Engineering 21, 427–431, (1982).
[27] Sutton, M. A., Wolters, W. J., Peters, W. H., Ranson, W. F., McNeill, S. R. “Determination of displacement using an improved digital correlation method,” Image and Vision Computation 1, 133–139, (1983).
[28] Zalevsky, Z., Beiderman, Y., Margalit, I., Gingold, S., Teicher, M., Mico, V., Garcia, J. "Simultaneous remote extraction of multiple speech sources and heart beats from secondary speckles pattern", Opt. Express, 17, 21566–21580, (2009).
[29] Li, L., Gubarev, F. A., Klenovskii, M. S., Bloshkina, A. I. "Vibration measurement by means of digital speckle correlation", In 2016 International Siberian Conference on Control and Communications (SIBCON) (pp. 1–5), IEEE, (2016).
[30] Hao, X., Zhu, D., Wang, X., Yang, L., Zeng, H. "A Speech Enhancement Algorithm for Speech Reconstruction Based on Laser Speckle Images". Sensors, 23(1), 330, (2023).
[31] Yoo, J. C., Han, T. H. "Fast normalized cross-correlation", Circuits, systems and signal processing, 28, 819–843, (2009).
[32] Di Stefano, L., Mattoccia, S., Tombari, F. "ZNCC-based template matching using bounded partial correlation", Pattern recognition letters, 26(14), 2129–2134, (2005).
[33] Kuglin, C. D., Hines, D. C. “The phase correlation image alignment method,” in Proc. IEEE 1975 Inf. Conf. Cybernet. Society, New York, No. 4, 163–165, (1975).
[34] Lewis, J. P. “Fast Template Matching”, Vision Interface, 120–123, (1995).
[35] Kim, S., Kim, J., Lim, W., Jeon, S., Kim, O., Koh, J. T., Kim, C., Choi, H., Kim, O. “In Vitro Bactericidal Effects of 625, 525, and 425 nm Wavelength (Red, Green, and Blue) Light-Emitting Diode Irradiation,” Photomed. Laser Surg. 31(11), 554–562, (2013).
[36] Sieuwerts, S., de Bok, F. A. M., Mols, E., de Vos, W. M., and van Hylckama Vlieg, J. E. T. “A simple and fast method for determining colony forming units”, Letters in Applied Microbiology, 47(4), 275–278, (2008).
[37] Loutfi, H., Pellen, F., Le Jeune, B., Lteif, R., Kallassy, M., Le Brun, G., Abboud, M., "Real-time monitoring of bacterial growth kinetics in suspensions using laser speckle imaging." Scientific Reports, 10(1), 408, (2020).
[38] Yoon J., Lee K., Park Y., “A simple and rapid method for detecting living microorganisms in food using laser speckle decorrelation,” arXiv:1603.07343, (2016).

[39] Murialdo, S. E., Sendra, G. H., Passoni, L. I., Arizaga, R., Gonzalez, J. F., Rabal, H., Trivi, M. “Analysis of bacterial chemotactic response using dynamic laser speckle,” J. Biomed. Opt. 14(6), 064015, (2009).
[40] Murialdo, S. E., Passoni, L. I., Guzman, M. N., Sendra, G. H., Rabal, H., Trivi, M., Gonzalez, J. F. “Discrimination of motile bacteria from filamentous fungi using dynamic speckle,” J. Biomed. Opt. 17(5), 056011, (2012).
[41] Kim, H., Singh, A. K., Bhunia, A. K., Bae, E. “Laser-induced speckle scatter patterns in Bacillus colonies,” Front. Microbiol. 5, 537, (2014).
[42] Grassi, H. C., García, L. C., Lobo-Sulbarán, M. L., Velásquez, A., Andrades-Grassi, F. A., Cabrera, H., Andrades-Grassi, J. E., Andrades, E. D."Quantitative Laser Biospeckle Method for the Evaluation of the Activity of Trypanosoma cruzi Using VDRL Plates and Digital Analysis," PLoS Negl. Trop. Dis. 10(12), e0005169, (2016).
[43] Grassi, H. C., Velásquez, A., Belandria, O. M., Lobo-Sulbarán, M. L., Andrades-Grassi, J. E., Cabrera, H., Andrades, E. D. “Biospeckle laser digital image processing for quantitative and statistical evaluation of the activity of Ciprofloxacin on Escherichia coli K-12,” Laser Phys. 29(7), p.075603, (2019).
[44] Zhou, K., Zhou, C., Sapre, A., Pavlock, J. H., Weaver, A., Muralidharan, R., Noble, J., Kovac, J., Liu, Z., Ebrahimi, A."Dynamic Laser Speckle Imaging meets Machine Learning to enable Rapid Antibacterial Susceptibility Testing (DyRAST)," ACS Sens. 5(10), 3140–3149, (2020).
[45] Váchová, L., Cáp, M., and Palková, Z. Yeast colonies: a model for studies of aging, environmental adaptation, and longevity. Oxid. Med. Cell. Longev., 601836, (2012).
[46] Lai, X., Torp, H. “Interpolation methods for time-delay estimation using cross- correlation method for blood velocity measurement. Ultrasonics, ferroelectrics, and frequency control,” IEEE Transactions 46(2), 277–290, (1999).
[47] Tukey, J. W. Nonlinear (nonsuperimposable) methods for smoothing data. Proc. Con. Rec. EASCON. 673, (1974).
[48] Jwo, D. J., Chang, W. Y., Wu, I. H., "Windowing techniques, the Welch method for improvement of power spectrum estimation", Comput. Mater. Contin, 67, 3983–4003, (2021).
[49] Nyquist, H., “Certain Topics in Telegraph Transmission Theory. Transactions of the American Institute of Electrical Engineers”, 47(2), 617–644, (1928).
[50] Shannon, C. E. “Communication in the presence of noise”, Proceedings of the Institute of Radio Engineers. 37 (1), 10–21, (1949).
[51] Rivas, E.-M., Gil de Prado, E., Wrent, P., de Silóniz, M.-I., Barreiro, P., Correa, E. C., Conejero, F., Murciano, A., and Peinado, J. M. "A simple mathematical model that describes the growth of the area and the number of total and viable cells in yeast colonies," Lett. Appl. Microbiol. 59, 594–603, (2014).
[52] Hoff, J., Daniel, B., Stukenberg, D., Thuronyi, B. W., Waldminghaus, T., and Fritz, G. "Vibrio natriegens: an ultrafast-growing marine bacterium as emerging synthetic biology chassis," Environ Microbiol. (2020).
[53] Lehmann, E. L. Theory of Point Estimation (Wiley, 1983).
[54] Pirt, S. J. "A kinetic study of the mode of growth of surface colonies of bacteria and fungi", J. Gen. Microbiol. 47(2), 181–197, (1967).
[55] Tenover, F. C., Antimicrobial Susceptibility Testing, 4th ed., 166–175 (Academic Press, 2019).

[56] Bonev, B., Hooper, J., Parisot, J. "Principles of assessing bacterial susceptibility to antibiotics using the agar diffusion method", J. Antimicrob. Chemother, 61, 1295–1301, (2008).
[57] Fick, A., Poggendorff's Annalen, 94, 59–86. and (in English) Phil.Mag. S.4, Vol. 10, 30–39, (1855).
[58] Tjandra, K. C., Ram-Mohan, N., Abe, R., Hashemi, M. M., Lee, J.-H., Chin, S. M., Roshardt, M. A., Liao, J. C., Wong, P. K., Yang, S. "Diagnosis of Bloodstream Infections: An Evolution of Technologies towards Accurate and Rapid Identification and Antibiotic Susceptibility Testing," Antibiotics 11, 511, (2022).
[59] Haykin, S. "Neural Networks and Learning Machines". Third Edition, Pearson Education, Inc., McMaster University, Hamilton, Chapter 1 and Chapter 4, (2009).
[60] Sun, X. X., Qu, W., "Comparison between mean filter and median filter algorithm in image denoising field", Applied Mechanics and Materials, 644, pp. 4112–4116, (2014).
[61] Ian, G., Yoshua, B., and Aaron, C. Deep learning: Adaptive computation and machine learning, Chapter 6, (2017).
[62] Thomas, A. J., Petridis, M., Walters, S. D., Gheytassi, S. M., Morgan, R. E. Two hidden layers are usually better than one. In Engineering Applications of Neural Networks: 18th International Conference, EANN 2017, Athens, Greece, August 25–27, 2017, Proceedings (pp. 279–290). Springer International Publishing, (2017).
[63] Yotov, K., Hadzhikolev, E., Hadzhikoleva, S., Cheresharov, S. Finding the optimal topology of an approximating neural network. Mathematics, 11(1), 217, (2023).
[64] Briers, J. D., Richards, G. J., He, X. W. Capillary blood flow monitoring using laser speckle contrast analysis (LASCA). J. Biomed. Opt., 4, 164–176, (1999).
[65] Abou Nader, C., Loutfi, H., Pellen, F., Le Jeune, B., Le Brun, G., Lteif, R., Abboud, M. Assessing white wine viscosity variation using polarized laser speckle: A promising alternative to wine sensory analysis. Sensors, 17(10), 2340, (2017).
[66] Abou Nader, C., Pellen, F., Roquefort, P., Aubry, T., Le Jeune, B., Le Brun, G., Abboud, M. Evaluation of low viscosity variations in fluids using temporal and spatial analysis of the speckle pattern. Opt. Lett. 41, 2521–2524, (2016).

Ilya Balmages was born in 1978 in Kyiv, Ukraine. He obtained a Bachelor's degree in Electrical and Power Systems Engineering from Sami Shamoon College of Engineering (SCE), Beer-Sheva, Israel, in 2000, and a Master's degree in Electro-Optical Engineering from Ben-Gurion University of the Negev (BGU), Beer-Sheva, Israel, in 2006.

From 2007 to 2018, he worked at the EORD company in Haifa, Israel. Since 2019, he has been working at Riga Technical University (RTU), where he has held the positions of scientific assistant and researcher. He is currently a researcher at Riga Technical University (RTU). His scientific interests are related to non-invasive methods for detecting microorganism activity and the classification of microbial behaviour using image and signal processing, as well as machine learning techniques.